6 Cohesion (Bonding) in Solids

6.1 Introduction

Solids often adopt well ordered crystalline structures with well defined lattice constants. Having discussed the many-body Hamiltonian of a solid and its calculation in some detail in previous chapters, it is now natural to ask why a given element chooses a particular crystal structure, and what kind of properties are connected with it. In particular, what types and strengths of forces, i.e. what bonds hold the solid together. This topic is called 'cohesion' and it is very much to do with the nature of chemical bonding in solids.
Just like in all previous chapters, we will restrict ourselves to the situation $T \approx 0$K, i.e. sufficiently low temperatures. This is because at higher temperatures, the properties of matter do not only follow from the total energy alone, but are also governed by other free energy contributions. Differing vibrational properties of different crystalline structures can induce structural phase transitions to other configurations upon heating. In fact most elements switch their crystal structure several times before they melt. Another issue is the configurational entropy e.g. due to defects such as vacancies interstials, and impurities. At low enough temperatures, however, the cohesive properties follow predominantly from the chemical binding in a perfect lattice, i.e. from the electrostatic interaction of the electron density with the ions and the ion-ion interaction. And this is what we will study in this chapter.
The central property of low temperature cohesion is the *cohesive energy* $E^{\rm coh}$, which is the energy needed to rip a sample apart into widely separated atoms. If $\{\mathbf{R}_I\}$denotes a set of structural parameters characteristic for a crystal lattice, and $\{\mathbf{R}_0\}$ represents their value at the equilibrium crystal structure (neglecting zero-point vibrations), we thus have

$$E^{\rm coh} \;=\; -\left(\frac{E(\{\mathbf{R}_0\})}{M} - \frac{E(\mathbf{R}_I\} \to \infty)}{M}\right). \tag{6.1}$$

Here E is the total energy of the solid (it has a negative value), and M the number of atoms in the crystal. Note that with this definition, the cohesive energy is a positive number. More generally, one could also say that the cohesive energy is the energy required to separate a solid into its elementary "building blocks". It is usually understood that these "building blocks" are the neutral atoms, but sometimes it can be more convenient to use molecules (e.g. N_2 for solid nitrogen) or ions (e.g. Na^+ and Cl^- for NaCl). By an appropriate correction for the molecular dissociation energy, or the ionization energy of the cation (energy to remove an electron) and the electron affinity of the anion (energy to add an electron), such numbers can always be translated into the cohesive energy with respect to neutral atoms, which is what we will use primarily. Cohesive energies of solids range from little more than a few meV per atom to just under 10 eV per atom, as can be

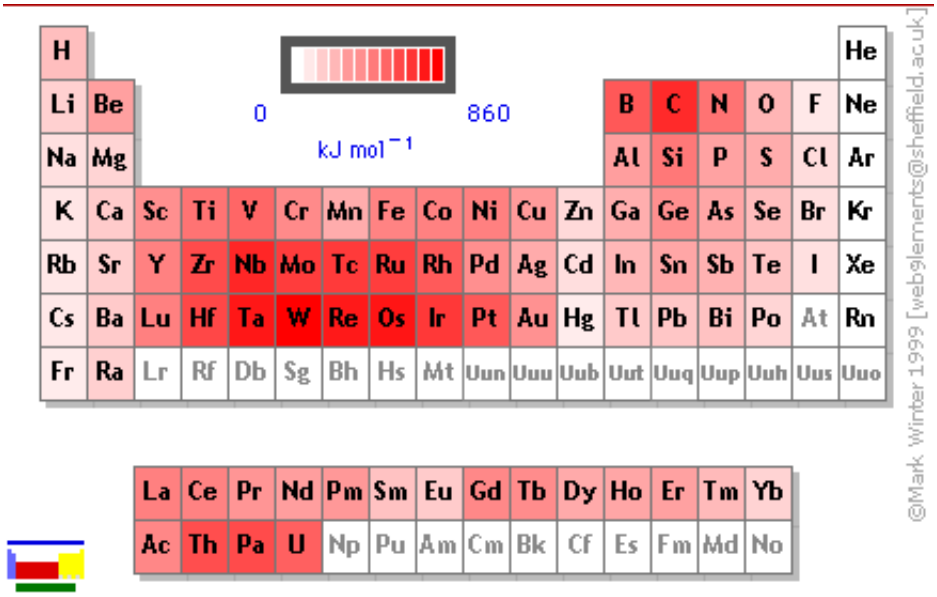

Figure 6.1: Experimental cohesive energy over the periodic table of elements (96 kJ/mole = 1 eV). [From Webelements].

seen from Fig.6.1.

We note in passing that by itself, the cohesive energy is not of overridding importance for the practical strength of a material. Resistance to scatches and fractures are critical quantities as well, and these are physically distinct from the cohesive energy. The question that knowledge of the cohesive energy makes possible to answer, is which crystal structure the solid will adopt, namely the one with the highest $E^{\rm coh}$ (which is nothing else but the system achieving its lowest total energy). With the electronic structure methods discussed in the preceding chapters, the straightforward approach to cohesion would therefore simply to compute the total energy of the crystal as a function of $\{\mathbf{R}_I\}$ for a given lattice structure. The energy lowering obtained at the minimum $\{\mathbf{R}_0\}$ then gives the cohesive energy achievable in this particular lattice structure (cf. also with Fig. 2 of chapter 1). Repeating this for all sorts of lattices would finally enable us to identify the one of the highest $E^{\rm coh}$ and this will be the equilibrium crystal structure at low temperatures.

Figure (6.2) shows how this works in practice. Here, the total energy of tungsten has been computed with density-functional theory (DFT-LDA) as a function of the unit-cell volume V (i.e. using this one variable to represent the set $\{\mathbf{R}_I\}$ for these high symmetry structures). The points are the actually calculated values for the fcc, the hcp, and the bcc crystal structure. In order to obtain reliable minimum values for these discrete sets of points (and also to reduce the inherent numerical noise), one usually interpolates the obtained curves with so-called *equation of state* functions, which are analytical functions derived from general thermodynamic considerations about the internal energy in the vicinity of the minimum. A popular form is due to Murnaghan (F.D. Murnaghan, Proc.

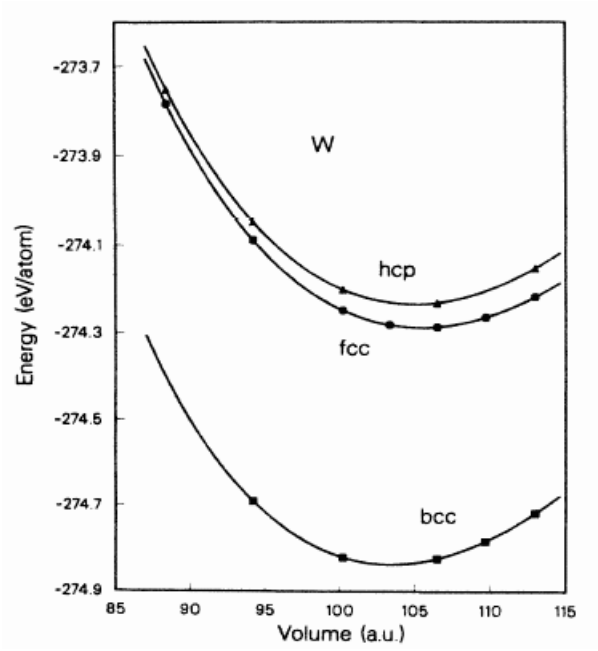

Figure 6.2: DFT-LDA total energy versus volume for W in the fcc, hcp and bcc structure. The bcc structure is the groundstate with the largest cohesive energy. [from C.T. Chan *et al.*, Phys. Rev. B **33**, 7941 (1986)].

Natl. Acad. Sci. U.S.A. **30**, 244 (1944)),

$$\frac{E(V)}{M} - \frac{E(V_0)}{M} = \frac{B_0 V}{B_0'(B_0'-1)}\left[B_0'\left(1-\frac{V_0}{V}\right) + \left(\frac{V_0}{V}\right)^{B_0'} - 1\right] \quad , \qquad (6.2)$$

which involves the following quantities

V_0: Volume at the energy minimum

B_0: Bulk modulus at V_o, as already defined in chapter 1. $B_0 = V\frac{\partial^2 E(V)}{\partial V^2}\Big|_{V=V_0}$

B_0': $= \frac{\partial B}{\partial p}\Big|_{V=V_0}$

Fitting V_0, B_0 and B_0' to the DFT data, the solid curves in Fig. 6.2 are obtained. We see that over quite a range of volumes this fit is perfect. In this particular case, the bcc structure is correctly obtained as ground state crystal structure of W, with an equilibrium lattice constant $a_0 = (2V_0)^{\frac{1}{3}} = 3.13\,\text{Å}$ and a bulk modulus $B_0 = 3.33\,\text{Mbar}$, which compare well to the experimental values of 3.16 Å and 3.23 Mbar, respectively. Also, the agreement of the derived $E^{\text{coh}} = 9.79\,\text{eV}$ (exp: 8.90 eV) with experiment is reasonable though not perfect. In fact, the significant overbinding obtained (too high cohesive energy and slightly too short bond length) is typical for the employed LDA functional, and partially corrected in present day GGA functionals. Note also, that less symmetric structures with a more atom basis often require a more extended set of $\mathbf{R}_I$ than just one parameter. One then has to compute the total energy as a higher dimensional function, e.g. of a and

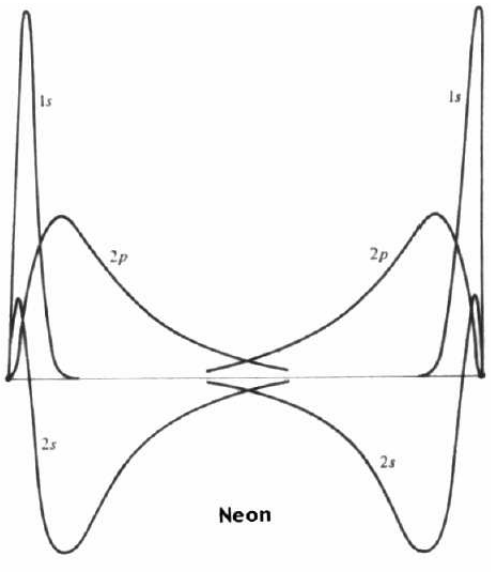

Figure 6.3: Radial atomic wave functions of two neon atoms at the equilibrium interatomic distance. Since the distance is relatively large, there is hardly any overlap of the wavefunctions [from Ashcroft and Mermin].

c (in plane and out of plane lattice constant) for the hcp structure.

A similarly precise or even more precise description of the cohesive properties as obtained for tungsten (Fig. (6.2)) can be achieved by present day DFT calculations for most elemental and compound solids. With this, we could in principle already close the chapter on cohesion. The level of accuracy we have achieved in describing the electronic interactions in solids seems enough to also fully explain the ensuing cohesive properties. Yet, although it is quite gratifying to have reached such a high degree of quantitative modeling with nowadays routinely employed electronic structure theories, this would still leave us somewhat unsatisfied. Because what we have not yet gained is *understanding* of *why* the bcc structure is actually the most favored one for W, and *why* the cohesive energy has roughly the value it has. Even more important, we would also like to understand, why the cohesive energy and equilibrium crystal structure exhibit certain trends over the periodic system of elements as exemplified in Fig. 6.1.

Such an understanding has typically been developed by discussing five idealized types of bonding: *i) van der Waals; ii) ionic; iii) covalent; iv) metallic;* and *v) hydrogen bonding.* Almost no real solid can be classified 100% into any one of these five categories nevertheless it has proven useful to make this division to gain a qualitative understanding of the largely varying cohesive properties of solids. Indeed this is how we shall proceed by introducing each of the five 'types' of bond that hold solids together; focusing particular on common examples from each category and, where possible, providing simple intuitive models by which each type of bond can be understood.

6.2 Van der Waals Bonding

Before we discuss this type of bonding we shall point out that physicists and chemists have, for the most part, two different definitions for what a van der Waals bond actually is. The International Union of Pure and Applied Chemistry (IUPAC) - the authority on nomenclature, definitions, etc. in chemistry - defines a van der Waals bond as *'the at-*

tractive or repulsive forces between molecular entities (or between groups within the same molecular entity) other than those due to bond formation or to the electrostatic interaction of ions or of ionic groups with one another or with neutral molecules. This term includes: dipole-dipole, dipole-induced dipole and London (instantaneous induced dipole-induced dipole) forces.' This definition persists largely for historical reasons; originally being used to explain the deviation of gases for ideal-gas behavior. This definition is *not* the standard definition of physics for a van der Waals bond. Specifically, in physics only the third of the three types of interaction listed, namely the induced dipole-induced dipole dispersive forces, constitute van der Waals bonding. In this lecture we shall, of course, use the physics definition that dispersive forces, the instantaneous induced dipole-induced dipole forces constitute van der Waals bonding. We are careful to stress this distinction because we will see that DFT does not describe the dispersive forces of van der Waals bonding correctly. It is however capable of treating the other types of interaction included in the *chemical* definition of van der Waals. So when it is said that DFT with state-of-the-art exchange-correlation functionals does not describe van der Walls bonding it is only the long-range tail of the dispersion forces that are not treated correctly.

The paradigm elements which are held together by van der Waals bonds are the noble gas atoms Ne, Ar, Kr, Xe (leaving out He which exhibits special properties due to its extremely light mass ensuing strong quantum-mechanical effects/zero-point vibrations). These are the elements that have filled valence shells. The two overriding features of van der Waals forces are that they are: i) non-directional; and ii) relatively weak (compared to the other types of bonding that we shall discuss).

Figure 6.3 illustrates the conceptual idea of van der Waals bonding using the example of two neon atoms. Noble gas atoms have filled shells, and there is a rather large energy gap to the lowest lying unoccupied states in the next shell. As soon as the wave functions of the two neon atoms start to overlap, electrons would need to go to these much higher states, since there are no free states in the shell left and the Pauli principle forbids two electrons in the same states (technically the wave functions need to orthogonalize, yielding new solutions with high energy). This occupation of high lying states costs a lot of energy, the total energy goes up, or in other words we have a strongly repulsive interaction. Obviously, this *Pauli repulsion* will always occur, when filled shells start to overlap. Ultimately, this is the mechanism responsible for the steep increase of the total energy in all bonding types at very small distances (as soon as the inner shells of the atoms start to overlap). The big difference with the rare gas atoms is that this happens already at relatively large distances, when the valence shells start to overlap, thereby preventing a closer approach of the two atoms. That there is an attractive interaction at all in this case is only due to small quantum mechanical fluctuations in the electron density of any of the two atoms. These give rise to momentarily existing dipoles, and although they average out over time, instantaneous electric fields are produced by them at any moment in time, inducing corresponding dipoles on the other atom. The interaction then results from the attraction between these two fluctuating dipoles.
Qualitatively we would therefore expect a variation of the total energy of the two atoms with distance R as shown in Fig. 6.4. At large distances there is a weak attraction and at small distances there is a strong repulsion, giving rise to a weak bonding minimum in between. For the attractive part, we can even derive the rough functional form based on

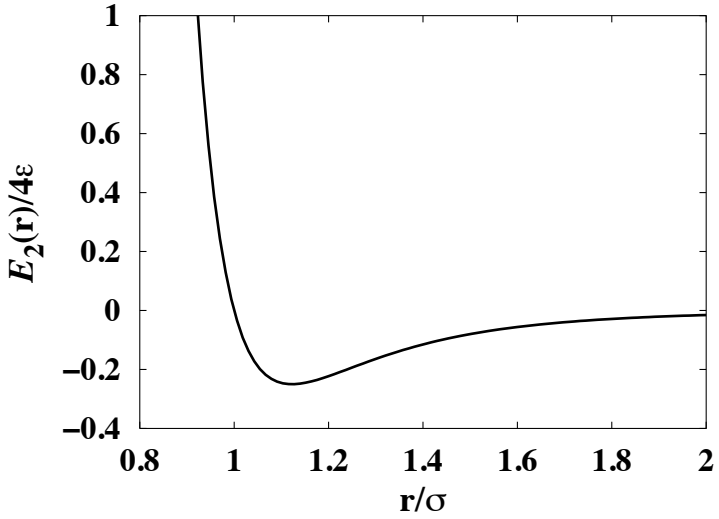

Figure 6.4: Lennard-Jones potential, cf. eq. (6.4), for the pair interaction between two noble gas atoms at distance R.

	T_b(°C)	$\alpha(10^{-24}$ cm $^3)$
He	-268.9	0.21
Ne	-246.1	0.40
Ar	-185.9	1.64
Kr	-153.2	2.48
Xe	-108.0	4.04
Rn	-61.7	5.30

Table 6.1: Compilation of the boiling temperatures and (static average) polarizabilities for the noble-gas elements. Data taken from the CRC handbook of Chemistry and Physics (78^{th} edition)

the above sketched understanding of interacting dipoles: The electric field connected to a dipole of dipole moment $\mathbf{P_1}$ is $\mathbf{E} \propto \frac{\mathbf{P_1}}{R^3}$. This field induces the dipole moment $\mathbf{P_2} = \alpha\mathbf{E} \simeq \alpha\frac{\mathbf{P_1}}{R^3}$ on the other atom, where α is the polarizability of the atom. The two dipoles $\mathbf{P_1}$ and $\mathbf{P_2}$ have then an interaction energy given by

$$\frac{\mathbf{P_1}\mathbf{P_2}}{R^3} \sim \frac{\alpha\mathbf{P_1}^2}{R^6} \quad , \tag{6.3}$$

i.e. we would roughly expect the attractive part to scale as $\sim -AR^{-6}$, where A is a proportionality constant, and the negative sign indicates attraction.

It is also clear from Eq. (6.3) that the van der Waals force between two species depends on polarizability (the susceptability of an atom or molecule to the formation of a dipole upon exposure to an electric field). Indeed this dependence nicely explains several trends, the most famous of which is the very variation in the boiling points of the noble gases. As one moves down the noble-gas series in the periodic table the polarizability increases (because the size of the elements increase) and so too does the boiling point of the element. See Table 6.1, for example, in which the boiling points and polarizability for the noble gases are listed.

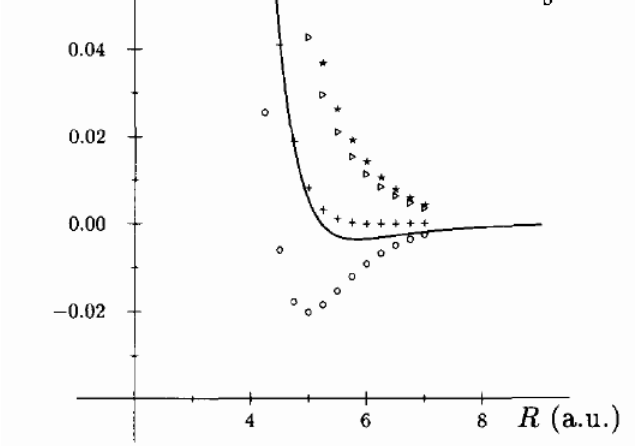

Figure 6.5: Total- energy curve for the Ne_2 molecule. The solid line is the result from an "exact" highest-order quantum chemistry calculation, exhibiting the correct shallow binding minimum. DFT-LDA (circles), on the other hand, significantly overestimates this binding, whereas the GGA (stars) gives a purely repulsive curve. The admixture of exact exchange to the GGA (crosses) gives results that are not too far off anymore [from J.M. Perez-Jorda and A.D. Becke, Chem. Phys. Lett. **233**, 134 (1995)].

Considering now the repulsive part due to the overlap of wavefunctions, an appealing choice for a functional form would be an exponentially increasing term (since atomic wavefunctions have exponentially decaying tails). However, historically a positive power law term $\sim BR^{-12}$ is rather used instead, leading in total to the so-called *Lennard-Jones 6-12 potential* shown in Fig. 6.4. Using the units $\sigma = (B/A)^{1/6}$ and $\varepsilon = A^2/4B$, its functional form is typically written as

$$E_2^{\mathrm{LJ}}(R) \;=\; 4\varepsilon \left\{ \left(\frac{\sigma}{R}\right)^{12} \;-\; \left(\frac{\sigma}{R}\right)^{6} \right\} \quad . \tag{6.4}$$

The precise form of the repulsive term is in fact not even that important. Any term with an inverse power higher than 6 would have done to yield a steeply rising energy at small distances. And as a note aside, there are in fact other frequently employed potential forms like the Born-Mayer potential that use an exponential for the hard-core repulsion.
With the Lennard-Jones potential, the complete interaction between two noble gas atoms is described by just two parameters (σ and ε). These can be obtained by fitting this curve either to experimental data from low-density gases (second virial coefficient) or to computed total-energy curves from highest order quantum-chemistry approaches. Both yield virtually identical results, which can be almost perfectly fitted by the functional form of the Lennard-Jones curve. For Ne_2 one obtains e.g. $\sigma = 2.74\,\text{Å}$ and $\varepsilon = 3.1\,\text{meV}$ [cf. e.g. N. Bernardes, Phys. Rev. **112**, 1534 (1958)] As we can see the parameters σ and ε conveniently provide a feel for the location of the minimum and the magnitude of its on the Lennard-Jones potential energy surface.

As we mentioned already the current workhorse in electronic structure theory calculations, DFT, has some problems with such very weakly binding van der Waals systems. This is ultimately connected with the fact that the presently employed functionals (like LDA or GGAs) contain only local exchange and correlation effects by construction. The dipole-dipole fluctuations responsible for the attractive part of the Lennard-Jones curve are, on the other hand, non-local in nature. This problem is usually simply summarized by saying that the current implementations of DFT are lacking the description of the long-range

behavior of van der Waals (or dispersion) forces. This issue is nicely explained in Fig. 6.5, again for the Ne_2 molecule. Why LDA (or to a better degree GGAs with exact exchange admixture) nevertheless give a bonding minimum is still controversially discussed. Figure 6.6, for example, illustrates how the addition of a van der Waals correction term to a commonly used GGA functional (the 'PBE' functional) yields a binding energy between two amino acids that is in much better agreement with experiment. These approaches whilst arguably of some use essentially amount to little more than an *a posteriori* correction. At present the appropriate and efficient treatment of van der Waals interactions is a very active field in density-functional theory. We have seen significant developments in recent years and more is expected to come. These developments also include terms that appear beyond the pairwise $\sim 1/R^6$ interactions.

Having understood the binding between two noble gas atoms, a straightforward way of describing the bonding in a noble gas solid would be to simply sum up the pairwise bonding contributions between all atoms in the solid. Since all atoms are equivalent, this corresponds to summing up the contributions from all other atoms as experienced by an arbitrary atom, which we take to be located at $\mathbf{R_1} = 0$. For the energy per atom we then obtain

$$\frac{E}{M} \simeq \frac{1}{2} \sum_{I=2}^{M} E_2^{\mathrm{LJ}}(|\mathbf{R_I}|) \quad , \tag{6.5}$$

where the factor $1/2$ corrects for double-counting. We immediately stress that considering only the (purely distance dependent) pair interaction is a gross simplification. In general, any additional particle will affect the electron density of all atoms in its neighborhood, and thereby also modify the pairwise interactions among the latter. This is exactly, why one needs in principle a new self-consistent calculation for each atomic configuration.

Expanding the total energy in terms of interactions between all particles, it can, however, be taken into account by including so-called three-body or even higher order many-body interactions. We will find such terms necessary in the other bonding classes, but for the noble gases the restriction to pairwise interaction is often sufficient, at least as a first step. As long as the particles do not approach each other too closely, the wave functions remain quite undisturbed from the form in the free atom. Adding more particles in the vicinity of other particles does therefore not affect the electron densities of the latter significantly, and correspondingly a pairwise sum is expected to describe the total energy quite well.

If we insert the exact form of the Lennard-Jones potential from eq. (6.4), we obtain for the energy per atom in the pair potential approximation

$$\frac{E}{M} = 2\varepsilon \sum_{I=2}^{M} \left\{ \left(\frac{\sigma}{|\mathbf{R}_I|} \right)^{12} - \left(\frac{\sigma}{|\mathbf{R}_I|} \right)^{6} \right\} \quad . \tag{6.6}$$

It is useful to rewrite this expression in a form, which allows one to evaluate the sum over all atoms in a general form for a given crystal structure. We therefore introduce the dimensionless quantity α_I,

$$|\mathbf{R}_I| = \alpha_I \cdot c, \tag{6.7}$$

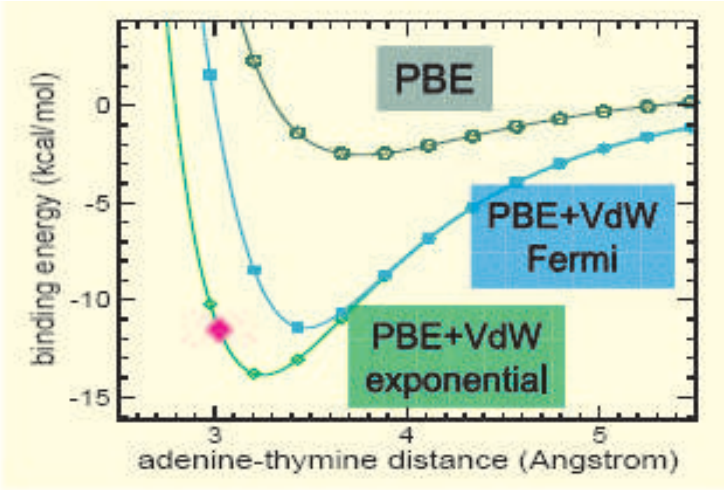

Figure 6.6: Binding energy as a function of separation for an adenine-thymine pair. A common GGA functional such as the 'PBE' functional does not capture the van der Waals binding energy between these molecules. This can be corrected *a posteroiri* by adding a van der Waals correction to the DFT total energy which then yields a binding energy in qualitative agreement with experiment (solid diamond). Binding energy curves for two functional forms of the van der Waals correction (exponential and Fermi function) are shown. For more details see Q. Wu and W. Yang, J. Chem. Phys. **116**, 505 (2002) [Courtesy of M. Fuchs].

where c is the distance to the nearest neighbor in the considered crystal structure. With this, the energy per atom can be written

$$\frac{E(c)^{\text{crystal}}}{M} \;=\; 2\varepsilon \left\{ \left(\frac{\sigma}{c}\right)^{12} A_{12}^{\text{crystal}} \;-\; \left(\frac{\sigma}{c}\right)^{6} A_{6}^{\text{crystal}} \right\} \quad . \tag{6.8}$$

The energy is then just a function of the nearest neighbor distance, and all the information about the particular crystal structure (i.e. number of neighbors in nearest, next-nearest etc. shells) is contained in the lattice sum

$$A_n^{\text{crystal}} \;=\; \sum_{I \in \text{crystal}} \alpha_I^{-n}. \tag{6.9}$$

As an illustration let us evaluate this lattice sum for the fcc crystal structure. In this lattice type we have 12 nearest neighbors at distance c ($= a_{\text{fcc}}/\sqrt{2}$, where a_{fcc} is the lattice constant). Then we have 6 next-nearest neighbors at a distance $\sqrt{2}c$, and so forth. Hence, the α_I for the first two shells are 1 and $\sqrt{2}$, cf. eq. (6.7). Obviously, for more distant neighbor shells, the α_I successively become larger, and correspondingly their contribution to the lattice sum smaller (inverse power). For A_{12}^{fcc} we arrive therefore at

$$A_{12}^{\text{fcc}} \;=\; 12 \cdot (1)^{-12} \;+\; 6 \cdot (\sqrt{2})^{-12} \;+\; \ldots \;=\; 12.13 \quad . \tag{6.10}$$

The lattice sum is thus already quite well approximated by only the first nearest neighbor shell. This is a consequence of the high power $n = 12$ considered in A_{12}. In fact, $A_{n\to\infty}$ is exactly given by the number of nearest neighbors (in this case the only non-zero term will

	sc	bcc	fcc
NN	6	8	12
A_6	8.40	12.25	14.45
A_{12}	6.20	9.11	12.13
$A_6^2/2A_{12}$	5.69	8.24	8.61

Table 6.2: Number of nearest neighbors, NN, and lattice sums for the three cubic Bravais lattices. The final row is proportional to the energy of the crystal. Further lattice sum values for other n can be found in Ashcroft/Mermin.

	Ne	Ar	Kr	Xe
c_0 (theory)	3.13 Å	3.75 Å	3.99 Å	4.33 Å
c_0 (exp.)	2.99 Å	3.71 Å	3.98 Å	4.34 Å
$E^{\rm coh}$ (theory)	27 meV	89 meV	120 meV	172 meV
$E^{\rm coh}$ (exp.)	20 meV	80 meV	110 meV	170 meV

Table 6.3: Equilibrium nearest neighbor distance c_0 and cohesive energy $E^{\rm coh}$ of the noble gases, as resulting from experiment and the pair potential approximation discussed in the text (theory). The larger deviation of c_0 for the lightest element Ne is due to zero-point vibrations, which are neglected in the theory [from Ashcroft and Mermin].

be the leading one). For lower n, on the other hand, the more distant neighbour shells contribute more significantly, as can be seen from Table 6.2.
From the general form of eq. (6.8) it is straightforward to deduce the equilibrium nearest neighbor spacing c_o and the cohesive energy for any given crystal structure,

$$\begin{aligned} \left.\frac{dE^{\rm crystal}(c)}{dc}\right|_{c_0} &= 0 \quad \Rightarrow \quad c_0 = \sigma \left(\frac{2A_{12}^{\rm crystal}}{A_6^{\rm crystal}}\right)^{1/6} \\ E^{\rm coh,crystal} &= -\frac{E^{\rm crystal}(c_0)}{M} = \varepsilon \frac{(A_6^{\rm crystal})^2}{2A_{12}^{\rm crystal}}. \end{aligned} \tag{6.11}$$

The cohesive energy for a particular element (entering only via ε) in a given crystal lattice therefore only the lattice sum, $\frac{(A_6^{\rm crystal})^2}{2A_{12}^{\rm crystal}}$. The lattice maximizing this sum will be the most stable one. Inspecting Table (6.2) we find that this is the case for the fcc structure. We have to note, however, that the hcp lattice has highly similar lattice sums (deviating only in the third digits). The crudeness of the approach does not allow to distinguish between such subtle differences. All we can conclude therefore is that van der Waals bonding will favor close packed lattice structures, which is ultimately a consequence of the underlying non-directional pair interaction.

All noble gases (except He) solidify indeed into an fcc structure. Using the parameters σ and ε obtained by fitting the Lennard-Jones curve to low-density gas phase data or the quantum-chemistry calculations of the diatomic molecules, we obtain the cohesive energies and lattice constants listed in Table 6.3. Considering the simplicity of our pair-potential model, the agreement is quite good (errors are roughly at the 10% level). At

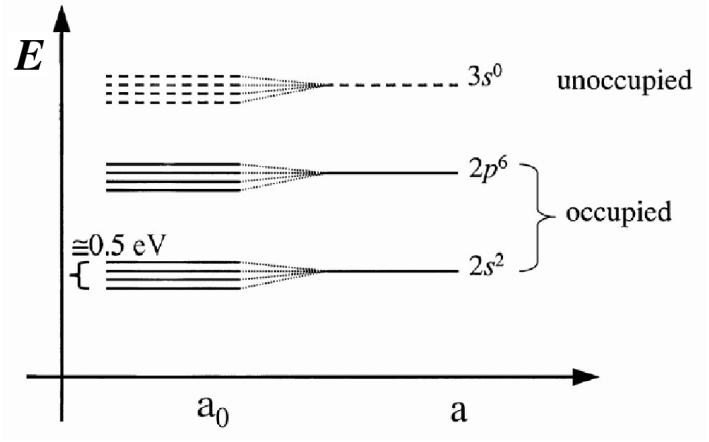

Figure 6.7: Sketch of the energy levels of a noble gas crystal, using the example of Neon. In the atomic limit a, all shells are filled. Even at the equilibrium lattice constant a_o the interaction between the atoms is weak, and the electronic states are only broadened by a small amount. This still leaves a large energy gap between occupied and unoccupied states, and Neon results as an insulator.

the obtained quite large equilibrium bond lengths, the wave function overlap is indeed minimal (as anticipated). The energy levels in a noble-gas solid will therefore show only a small broadening compared to the atomic limit as explained in Fig. 6.7. Due to the large energy difference between the uppermost occupied and the lowermost unoccupied band, rare gas crystals will behave as an insulator. On the basis of a crude pair potential we can thus understand quite some fundamental cohesive (and even electronic) properties of the noble metals solids. This is gratifying in this special case, but we will see that it is more an exception, than a rule.

6.3 Ionic bonding

Atoms and ions with closed shells are particularly stable, i.e. a lot of energy is required to excite an electron from a filled shell into an unoccupied state. The conceptual idea behind ionic bonding is therefore that electrons are exchanged in such a way, that the atoms involved reach this stable closed shell state. This is most easily realized for the so-called ionic crystals formed of alkali halides (i.e. Group I and VII elements of the periodic table). Take NaCl as an example. The conception then is, that Na with the electron configuration of $[1s^2 2s^2 2p^6]3s^1$ becomes a Na^+ ion, and Cl $[1s^2 2s^2 2p^6]3s^2 3p^5$ is turned into a Cl^- ion, thereby achieving the closed shell configuration in both cases. Similar ideas would, e.g., also hold for II-VI compounds. With this electron transfer accomplished, we arrive at a situation that is quite similar to the one discussed in the last section: the interaction between two filled shell ions. As soon as they come too close together (something that is now more determined by the ionic radii and not the atomic radii, though), hard core repulsion will set in. Contrary to the van der Waals case, the attractive interaction is, primarily due to the much stronger electrostatic attraction between the differently charged ions. If this electrostatic attraction is stronger than the cost of exchanging the electrons between the atoms to reach the ionic states, the crystal will hold together. Ionic bonding

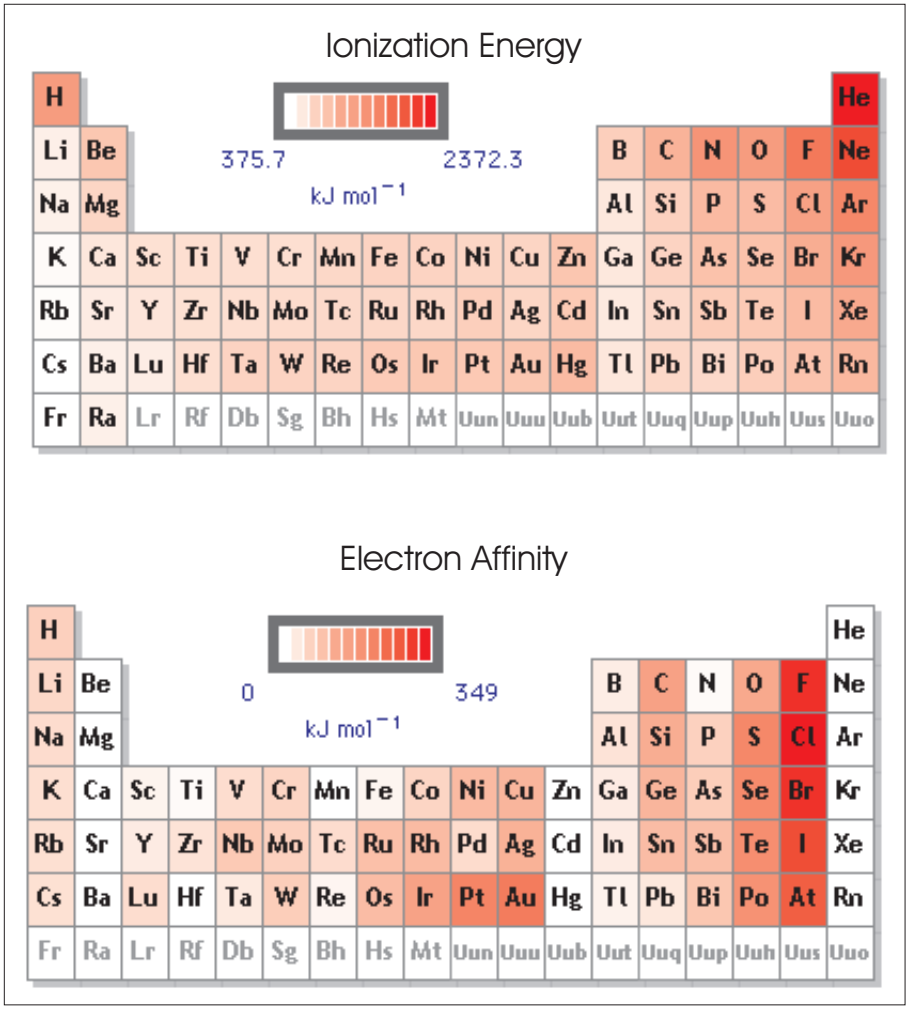

Figure 6.8: Periodic variation of the first ionization energies (top) and electron affinities (bottom) of the elements (96 kJ/mole = 1 eV) [From Webelements].

is therefore most effective, if the cost to create the ions is low, i.e. when one atom type readily gives away electrons (low ionization potential) and the other one readily takes them (high electron affinity). If one looks at Fig. 6.8 one sees that elements to the left of the periodic table, in particular in groups I and II tend to have the lowest ionization energies and elements to the right of the periodic table (groups VI and VII) tend to have the highest electron affinities. As a consequence ionic bonds are most common amongst binary solids containing these elements. Note that H is a clear exception to this trend. We will have more to say about this when discussing hydrogen bonding.

In this most naive perception an ionic crystal is simply a collection of impenetrable charged spheres, glued together by electrostatic interaction. In analogy to the van der Waals case, we thus expect the interaction between two ions of opposite charge to arise out of a repulsive and an attractive part. The repulsive part is due to Pauli repulsion, and since electrostatic interaction is much stronger than the (also existing) van der Waals forces,

Structure	A_{Mad}	NN
Cesium chloride	1.76	8
Sodium chloride	1.75	6
Wurtzite	1.64	4
Zincblende	1.64	4

Table 6.4: Madelung constants A_{Mad} and nearest-neighbor coordination NN for the most common ionic crystal structures.

the attractive part will be predominantly given by a Coulomb $1/R$-potential

$$E_2^{\mathrm{ionic}}(R) \;=\; E^{\mathrm{rep.}} + E^{\mathrm{attr.}} \;=\; \frac{C}{R^{12}} - \frac{e^2}{4\pi\varepsilon_o\, R} \quad , \tag{6.12}$$

where we have simply taken the charge on the ions as $\pm e$, and $\varepsilon_0 = 8.85 \cdot 10^{-12}\,\mathrm{As/Vm}$ is the vacuum dielectric constant. Note, that evaluating the constants in the attractive term leads to $E^{\mathrm{attr.}} = -14.4\,\mathrm{eV}/R$ [in], i.e. bringing the two ions together at a distance of 3 Å yields already about 4.5 eV electrostatic energy gain. The cost to create Na^+ and Cl^- (difference of electron affinity and ionization potential) is only $\sim 1.5\,\mathrm{eV}$, leaving still quite a lot of energy gain to form a very stable ionic bond. Just like in the van der Waals case, one has to recognize that the $1/R^{12}$ repulsive potential is only a rough and convenient choice. One can determine the proportionality constant C by fitting either to first-principles calculations or to experimental compressibility data. One then often finds, that using smaller inverse powers somewhere in the range 6-10 or an exponential form (Born-Mayer potential) can fit the data even better. For the general discussion on the chemical bonding intended here, such multiparameter fits are, however, not very illuminating, and we will stick for simplicity to the $1/R^{12}$-potential already used in the van der Waals case.

Having obtained the interaction between an ion pair, we may employ the same reasoning as in the last section to determine the cohesive energy of an ionic solid. Again, we do not expect dramatic charge rearrangements in the solid compared to the case of the isolated (closed-shell) ions. A simple sum over the pairwise contributions as in eq. (6.5) should therefore already describe the energy per ion pair quite well. This leads to

$$\frac{E}{M} \;\simeq\; \frac{1}{2}\sum_{I=2}^{M} E_2^{\mathrm{ionic}}(|\mathbf{R_I}|) \;=\; \sum_{I=2}^{M}\left\{\frac{C}{R_I^{12}} - \frac{\pm 1}{4\pi\varepsilon_o\, R_1}\right\} \quad , \tag{6.13}$$

where the ± 1 applies when the ion I in the sum has negative or positive charge, respectively. As before, we proceed by eliminating the properties exclusively due to the crystal structure through the definition of the dimensionless quantity α_I (cf. eq. (6.7)) and arrive at

$$\frac{E(c)^{\mathrm{crystal}}}{M} \;=\; \left\{\frac{C}{c^{12}} A_{12}^{\mathrm{crystal}} \;-\; \frac{e^2}{4\pi\varepsilon_0\, c} A_{\mathrm{Mad}}^{\mathrm{crystal}}\right\} \quad . \tag{6.14}$$

Similar to the lattice sums A_n^{crystal} defined in eq. (6.9), the complete information about the neighbor shells of ions with positive or negative charges in the particular crystal structure are now summarized in the so-called *Madelung constant*

$$A_{\mathrm{Mad}}^{\mathrm{crystal}} \;=\; \sum_{I\in\mathrm{crystal}} \frac{\pm 1}{\alpha_I}. \tag{6.15}$$

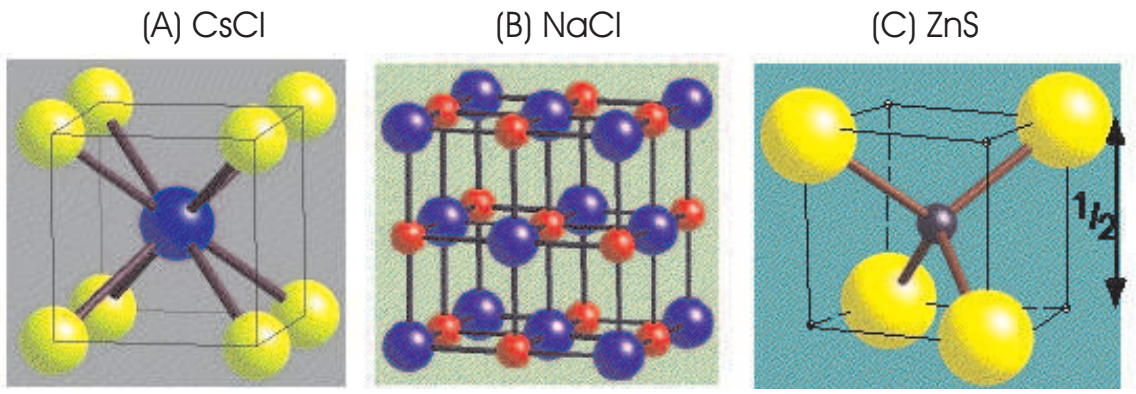

Figure 6.9: The two most common ionic crystal lattices: (A) Cesium chloride and (B) Sodium chloride; and (C)the less common zinc blende structure.

Apparently, this Madelung constant is the analog of the lattice sum A_1^{crystal}, taking additionally into account that neighboring ions with positive or negative charge contribute differently to the electrostatic interaction in the lattice. The weak decrease (or long range) of the $1/R$ potential makes the actual calculation of Madelung constants more tricky than to the one of lattice sums. Depending on the way the summation is carried out, any value whatsoever can be obtained (corresponding to finite crystals with differing surface charges). The method of choice to avoid such problems is the *Ewald summation* technique already discussed in section 1.3. With this, the Madelung constants of any crystal lattice can readily be computed and Table 6.4 lists a few A_{Mad} for lattice types that will become relevant in the discussion below.

From the structure of eq. (6.14) it is obvious that again the maximum cohesive energy will be obtained by close-packed structures, which maximize both the lattice sum A_{12} and the Madelung constant. As already noted in the last Section, this follows simply from the non-directional bonding implied by the interionic pair potential $E_2^{\text{ionic}}(R)$. Since the nearest neighbor shell contributes most strongly to A_{12} *and* A_{Mad}, but only ions of opposite charge yield electrostatic attraction, ionic crystals will more specifically prefer those close-packed structures in which each ion is surrounded by a shell of ions with opposite charge. Fig. 6.9 shows the two crystal structures that fulfill these close-packing and opposite ion shell requirements to an optimum. The sodium chloride (rocksalt) structure consists of two interpenetrating fcc lattices, thus achieving a coordination of 6 per ion, while the cesium chloride structure can be viewed as a bcc lattice with the ion of second type inhabiting the interior of the cube (coordination 8).

Table 6.4 lists the Madelung constants and coordination numbers of these two, and two less dense lattices (zincblende and wurtzite). As already discussed in the context of the lattice sum A_1, the Madelung constant is expected to scale with the coordination number, but not as clearly as for example A_{12}. The contribution of second and further neighbors is still significant, leading to highly similar Madelung constants for the 8-fold and 6-fold coordinated CsCl and NaCl lattices (only the 4-fold coordinated zincblende and wurtzite structures exhibit a noticeably lower A_{Mad}).

Leaving aside this influence on the specific crystalline arrangement chosen, the dominant contribution to the cohesive energy comes in any case from the electrostatic interaction (also often called Madelung energy E^{Mad}). This can be discerned by evaluating it at the

Compound	c_0(exp)	-E^{Mad}	E^{coh}(theory)	E^{coh}(exp)
LiF	2.01 Å	11.81 eV	10.83 eV	11.45 eV
LiCl	2.57 Å	9.65 eV	8.85 eV	8.98 eV
LiBr	2.75 Å	9.28 eV	8.51 eV	8.39 eV
LiI	3.01 Å	8.64 eV	7.92 eV	7.66 eV
NaF	2.32 Å	10.49 eV	9.62 eV	9.96 eV
NaCl	2.82 Å	8.32 eV	8.18 eV	8.18 eV
NaBr	2.99 Å	8.52 eV	7.81 eV	7.72 eV
NaI	3.24 Å	7.39 eV	7.32 eV	7.13 eV

Table 6.5: Experimental lattice constants c_o, Madelung electrostatic energies E^{Mad}, theoretical cohesive energies per (charged) ion pair E^{coh}(theory), cf. eq. (6.16), and experimental cohesive energies per ion pair E^{coh}(exp) for a number of alkali halides crystallizing in the sodium chloride lattice. The larger the ionic radii, the larger the lattice constant, and accordingly the lower the cohesive energy becomes. The largest part to the cohesive energy comes indeed from the electrostatic Madelung energy.

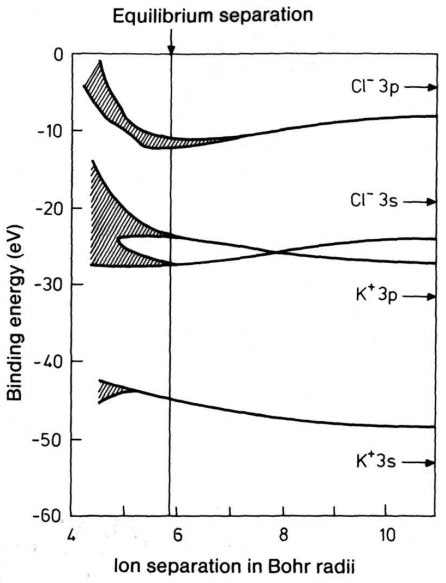

Figure 6.10: Calculated energy levels of a KCl-crystal as a function of the interionic distance d (measured in Bohr radii, a_o). The vertical line is the experimental value, and the ionic levels are indicated by arrows on the right-hand side. The valence band derives from the full Cl $3p$ shell, and at the experimental lattice constant a noticeable, but still small level broadening is discernible [from H. Ibach and H. Lu̇th, *Solid State Physics*, original source: L.P. Howard, Phys. Rev. **109**, 1927 (1958)].

experimentally determined lattice constant c_o. Using a strategy as in eqs. (6.11), one finds furthermore that the cohesive energy at this experimental lattice constant is

$$E^{\mathrm{coh,crystal}} \;=\; -\,\frac{E^{\mathrm{crystal}}(c_0)}{M} \;=\; -\frac{11}{12}\,E^{\mathrm{Mad}}(c_0) \;=\; \frac{11}{12}\frac{A_{\mathrm{Mad}}e^2}{4\pi\varepsilon_0 c_0} \quad . \tag{6.16}$$

Table 6.5 lists this energy and the Madelung energy for a number of alkali halides, and compares with experiment. The agreement is not as good as the one obtained in the previous section for the vdW bonded crystals, but given the simplicity of the theoretical model, it is clear that the essential physics are contained in it. The remaining 10-20% of the binding comes from overlapping and hybridized wave functions, which is for example reflected in the noticeable broadening of the energy levels as shown for KCl in Fig. 6.10. Still, the broadening is still much smaller than the separation between the individual levels, and consequently the alkali halides are insulators. Again, the only small overlap of the ionic charge distributions and correspondingly small charge rearrangements compared to the isolated ions, is the reason why the primitive pair potential approach works so well for these systems. A few other interesting relationships can be seen in Table 6.5: First, E^{Mad} is generally larger than E^{coh} which reflects the obvious existence of some repulsive energy at equilibrium; Second, E^{coh} is inversely proportional to lattice constant, which is what we would expect based on the 1/r dependence of the Madelung energy. Further discussions on these aspects can be found in J.A. Majewski and P. Vogl, Phys. Rev. Lett. **57**, 1366 (1986); Phys. Rev. B **35**, 9666 (1987).

This crude pair potential model can even be extended to explain semi-quantitatively some structural trends exhibited by ionic solids. In this context we introduce Pauling's so called *radius ratio rules*. Very briefly these relate the relative size of the anion and cation in a crystal (ionic radii can be determined by experiment with, for example, x-ray diffraction) to the preferred structure which is adopted. Specifically these state the intervals within which various structures are likely to occur:

$$1 > \frac{R+}{R-} > 0.73 \;(CsCl\ structure) \tag{6.17}$$

$$0.73 > \frac{R+}{R-} > 0.41 \;(NaCl\ structure) \tag{6.18}$$

$$0.41 > \frac{R+}{R-} > 0.23 \;(ZnS\ structure) \tag{6.19}$$

The relationships as listed here are merely based on the most efficient ways of packing different sized spheres in the various crystal structures. They can be easily verified with a few lines of algebra. The essential messages to take from these relationships are basically: (i) If the anion and cation are not very different in size then the CsCl structure will probably be favored: (ii) If there is an extreme disparity in their size then the ZnS structure is likely; and (iii) if in between the NaCl structure is likely.

Of course atoms are much more than just hard spheres but nonetheless correlations such as those predicted with these simple rules are observed in the structures of many materials. A partial understanding of why this is so can be obtained by simply plotting E^{Mad} as a function of the anion-cation ratio. This is done in Fig. 6.11. If, for example, one looks at the CsCl to NaCl transition in Fig. 6.11 it is clear that there is a discontinuity at 0.73 after which the Madelung energy remains constant. This transition is a consequence of the fact that the volume of the CsCl structure is determined solely by the second nearest

neighbour anion-anion interactions. Once adjacent anions come into contact no further energy can be gained by shrinking the cation further. It would simply "rattle" around in its cavity with the volume of the cell and thus the Madelung energy remaining constant. Further discussion on this issue and these simple *rules of thumb* can be found in Pettifor, *Bonding and Structure of Molecules and Solids*.

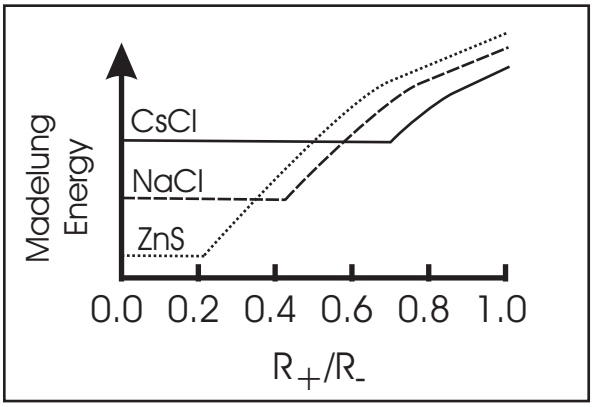

Figure 6.11: The Madelung energy in ionic compounds as a function of the radius ratio for CsCl, NaCl and cubic ZnS lattices (assuming the anion radius is held constant) (Based on Pettifor, *Bonding and Structure of Molecules and Solids*).

6.4 Covalent bonding

The ionic bonding described in the last section is based on a complete electron transfer between the atoms involved in the bond. The somewhat opposite case (still in our idealized pictures), i.e. when chemical binding arises out of electrons being more or less equally shared between the bonding partners, is called *covalence*. Contrary to the ionic case, where the electron density in the solid does not differ appreciably from the one of the isolated ions, covalent bonding results from a *strong overlap of the atomic-like wavefunctions of the different atoms*. The valence electron density is therefore increased *between* the atoms, in contrast to the hitherto discussed van der Waals and ionic bonding types. It is intuitive that such an overlap will also depend on the orbital character of the wavefunctions involved, i.e. in which directions the bonding partners lie. Intrinsic to covalent bonding is therefore a strong *directionality* as opposed to the non-directional ionic or van der Waals bonds. From this understanding, we can immediately draw some conclusions:

- When *directionality matters*, the preferred crystal structures will not simply result from an optimum packing fraction (leading to fcc, hcp or CsCl, NaCl lattices). The classic examples of covalent bonding, the group IV elements (C, Si, Ge) or III-V compounds (GaAs, GaP), solidify indeed in more open structures like diamond or zincblende.

- Due to the strong directional bonds, the displacement of atoms against each other (shear etc.) will on average be more difficult (at least more difficult than in the case of metals discussed below). Covalent crystals are therefore quite brittle.

Element		a_o (Å)	E^{coh} (eV/atom)	B_o (Mbar)
C	theory	3.602	7.58	4.33
	exp.	3.567	7.37	4.43
	%diff.	**<1%**	**3%**	**−2%**
Si	theory	5.451	4.67	0.98
	exp.	5.429	4.63	0.99
	%diff.	**<1%**	**1%**	**−1%**
Ge	theory	5.655	4.02	0.73
	exp.	5.652	3.85	0.77
	%diff.	**0.2%**	**4%**	**−5%**

Table 6.6: Comparison between DFT and experimental results for structural and cohesive properties of group IV semiconductors in the diamond structure. a_o lattice constant, E^{coh} cohesive energy, and B_o the bulk modulus [from M.T. Yin and M.L. Cohen, Phys. Rev. B **24**, 6121 (1981)].

- Directionality can not be described by only distance-dependent pair potentials. A theory of cohesion in covalent crystals will therefore be significantly more involved than the crude pair-potential approach that we found so successful to describe van der Waals and ionic crystals. In the language of interatomic potentials, there will be no way around introducing at least threebody, if not higher many-body terms. In fact, the common theme of interatomic potentials for covalent crystals, like the famous Stillinger-Weber potentials or the ubiquitous force-fields, are three-body terms that take angular components into account. Even then, the success and value of using such potentials is completely different compared to the pair potentials of the last two sections: For the latter we found that one general form can treat quite a range of situations and elements very well. Even for the best covalent interatomic potentials currently on the market, this *transferability* is very much limited. Although there are parametrizations that can describe one bonding situation for one element extremely well (say Si bulk), they completely fail for another element or for the same element in a different bonding environment (say Si surface). This reflects the fact, that the functional forms employed cannot embrace the changing character of the hybridizing wave functions, or in other words that one needs to explicitly treat the quantum mechanics of the electrons achieve a trustful descriptionand understanding. Interatomic potentials are nevertheless frequently (often unfortunately uncritically) employed in materials science research, and quite some effort is dedicated to developing further, improved functional forms that might exhibit a higher transferability and reliability. For our general discussion on bonding and cohesion, such refined potential approaches are, however, not very helpful.

Lacking a model of cohesive energy of comparable simplicity to those of van der Waals or ionic bonding, we have to stick to the more elaborate electronic structure theory descriptions as obtained e.g. with DFT. Fortunately, the latter does at least a remarkably good job in describing covalent crystals, as exemplified for the group IV semiconductors in Table 6.6. Recalling that there is no free parameter in the theory, the agreement is indeed quite impressive and shows that the current exchange-correlation functionals capture most of the essential physics underlying covalent bonding.

The requirement for quantitative calculations does not, however, necessarily prevent us from still attempting to gain some further conceptual understanding of the cohesive properties of covalent crystals. A useful concept for understanding some of the structures and properties of covalent materials both in solids and molecules is hybridization. Let's now have a quick look at this.

6.4.1 Hybridization

The formation of hybrid orbitals (or hybridization) has proved to be an extremely helpful and instructive concept for understanding the structure and bonding in many covalent materials (solids and molecules). Here we shall introduce the basic ideas of hybrid orbital formation with one or two instructive examples.
Let's consider carbon, which has the valence shell configuration $2s^2, 2p^2$. It is possible to make linear combinations of these four valence orbitals to yield a new set of hybrid orbitals. The resulting so-called *sp^3-hybrid functions* are

$$\phi^1 = \frac{1}{2}(s + p_x + p_y + p_z) \tag{6.20}$$

$$\phi^2 = \frac{1}{2}(s + p_x - p_y - p_z) \tag{6.21}$$

$$\phi^3 = \frac{1}{2}(s - p_x + p_y - p_z) \tag{6.22}$$

$$\phi^4 = \frac{1}{2}(s - p_x - p_y + p_z) \quad . \tag{6.23}$$

These correspond to the orbitals of an excited state of the atom, i.e. this set of hybrid orbitals is less stable than the original set of atomic orbitals. However, in certain circumstances it is possible for these orbitals to bond more effectively with orbitals on adjacent atoms and in the process render the composite (molecule, solid) system more stable. As shown in Fig. 6.12 the four sp^3 orbitals point to the four corners of a tetrahedron. This implies that sp^3 hybrid orbitals favor bonding in which atoms are tetrahedrally coordinated. Indeed, they are perfectly suited for the diamond structure, and the energy gain upon chemical bonding in this tetrahedral configuration outweighs the energy that is required initially to promote the s electrons to the p levels. Carbon in the diamond structure crystalizes like this as do other elements from group IV (eg. Si and Ge) and several III-V semiconductors. Some examples of the band structures of these covalent materials are shown in Fig. 6.13.
Although essentially just a mathematical construct to change basis functions the concept of hybridization can be rather useful when seeking qualitative understanding of different systems. For example, hybridization can be used to explain the qualitative trend in the size of the band gap in tetrahedral (group IV) semiconductors. In C, Si, Ge and Sn for example the splitting between the valence s and p shells are all approximately 7.5 eV. In the solid, however, the measured gaps between the valence and conduction bands are: C = 5.5 eV, Si = 1.1 eV, Ge = 0.7 eV, Sn = 0.1 eV. This trend can be understood through sp^3 hybrid formation in each element, which in the solid leads to sp^3 bonding (valence) and sp^3 antibonding (conduction bands). The width of the bonding and antibonding bands, and hence the band gap, depends upon the overlap between atoms in each solid, which of course is related to the 'size' of the individual elements. Carbon (in the diamond structure) therefore exhibits the largest band gap and Sn the smallest (See Fig. 6.14).

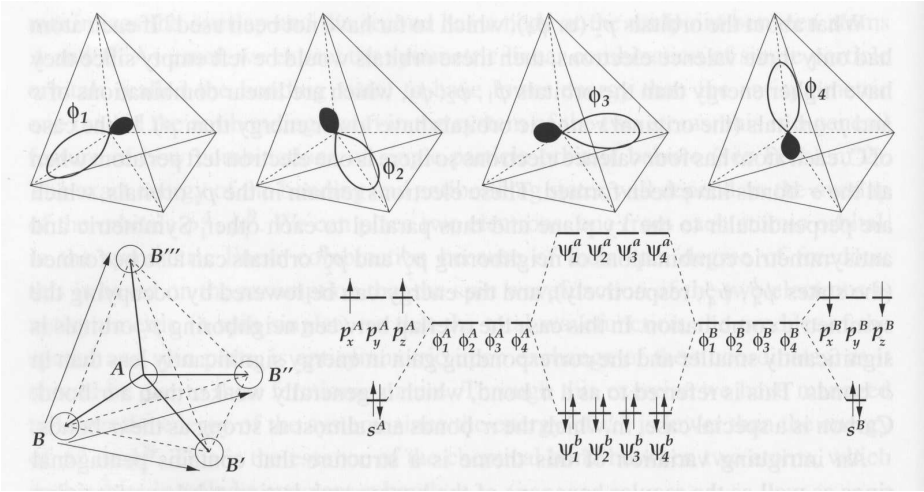

Figure 6.12: Illustration of the formation of sp^3 hybrid orbitals in C (from E. Kaxiras, *Atomic and Electronic Structure of Solids*).

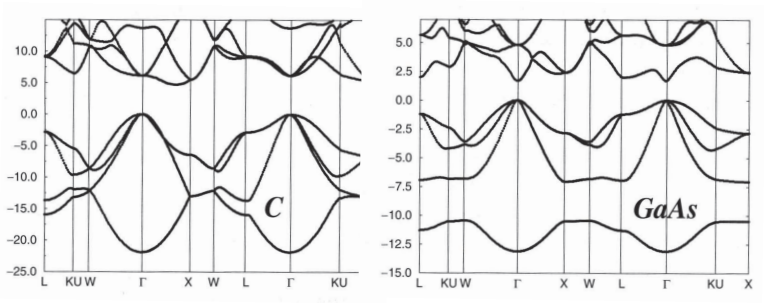

Figure 6.13: Band structures for some typical covalent materials in the diamond (C) and zinc blende (GaAs) structures. Both materials exhibit a ("hybridization") band gap (from E. Kaxiras, *Atomic and Electronic Structure of Solids*).

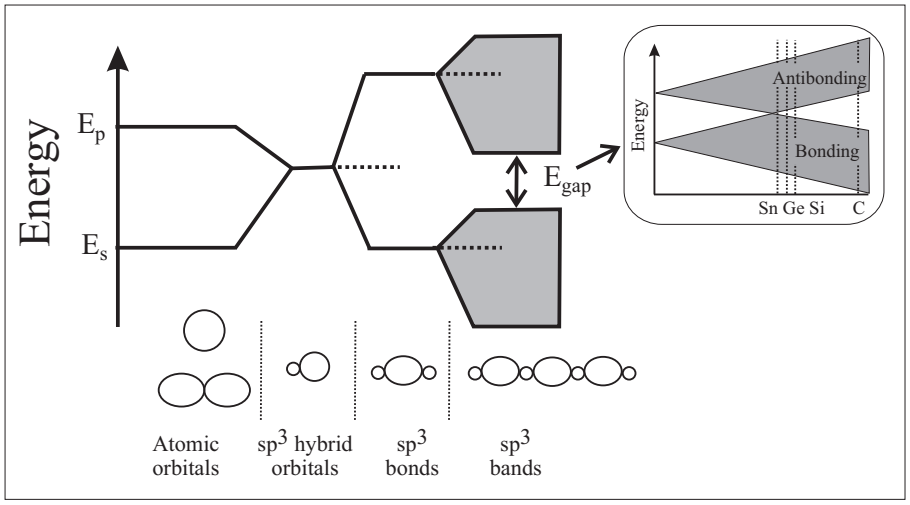

Figure 6.14: Illustration of the formation of sp^3 valence and conduction bands in the tetrahedral semiconductors. In the inset a schematic illustration of the opening up of the hybridization band gap in the energy bands of these solids. As one goes from C to Si to Ge to Sn the size of the atoms increase, which increases the band widths and decreases the band gap (after Pettifor).

Whereas this picture of sp^3-hybrids renders the high stability of the diamond structure and its high p valence character comprehensible, there is unfortunately no simple rule that would predict, which hybrid orbital set (and corresponding structure) is most preferred for each element. Hybrid orbital formation mainly provides a suitable *language* for describing the bonding properties of solids (and molecules). Indeed another common set of hybrid orbitals are the sp^2 set, which are often used to discuss layered structures:

$$\phi^1 = \frac{1}{\sqrt{3}}s + \frac{\sqrt{2}}{\sqrt{3}}p_x \tag{6.24}$$

$$\phi^2 = \frac{1}{\sqrt{3}}s - \frac{1}{\sqrt{6}}p_x + \frac{1}{\sqrt{2}}p_y \tag{6.25}$$

$$\phi^3 = \frac{1}{\sqrt{3}}s - \frac{1}{\sqrt{6}}p_x - \frac{1}{\sqrt{2}}p_y \tag{6.26}$$

$$\phi^4 = p_z \quad . \tag{6.27}$$

An illustration the sp^2 hybrid orbitals and their resultant energy levels for C is shown in Fig. 6.15. It can be seen that sp^2 hybrid formation is compatible with bonding in a trigonal arrangement (bonding in a plane with an angle of 120° between neighbours. For C in the solid state this gives rise to graphite, which contains a combination of strong in-plane σ and π sp^2 derived bonds and much weaker interlayer (van der Waals) bonds. Finally, we should stress that the initially mentioned view of ionic and covalent bonding as opposite extremes indicates already, that most real structures will exhibit varying degrees of both bonding types. This is nicely illustrated by the series Ge, GaAs, and ZnSe, i.e. a pure group IV, a III-V and a II-V structure all in the same row of the periodic system of elements. Fig. 6.16 shows the corresponding valence electron densities. While the increased

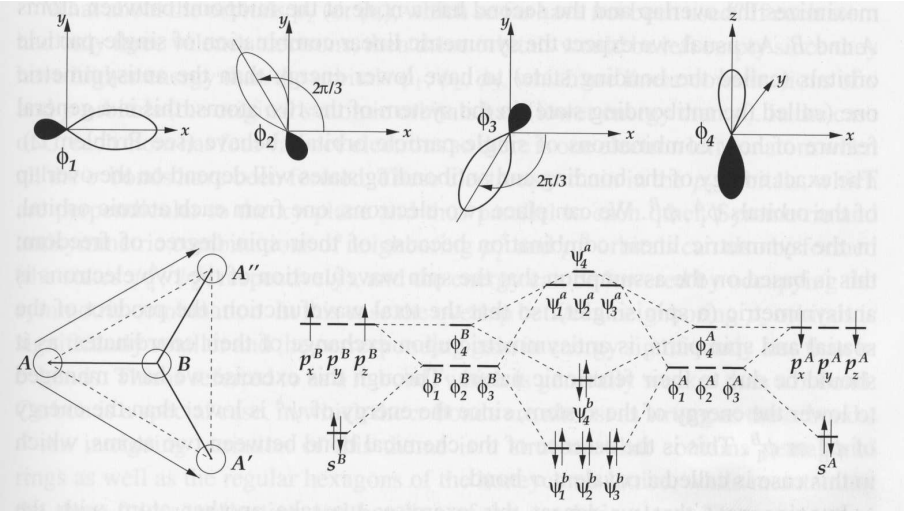

Figure 6.15: Illustration of the formation of sp^2 hybrid orbitals in C (from E. Kaxiras, *Atomic and Electronic Structure of Solids*).

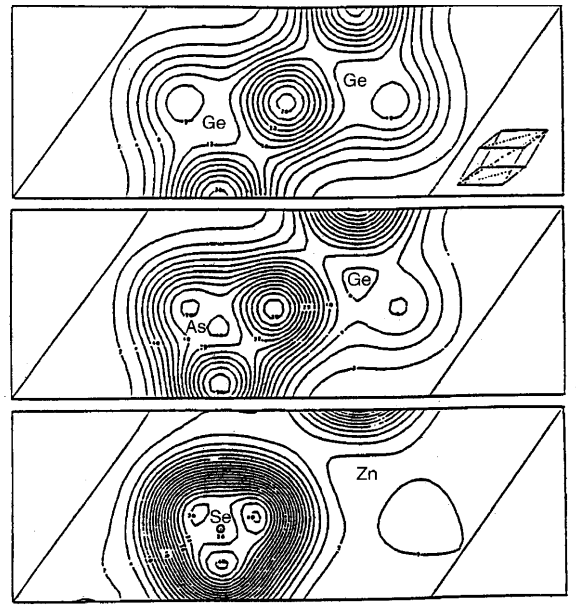

Figure 6.16: Valence electron density of Ge (top), b) GaAs (middle), and c) ZnSe (lower) in e per unit-cell volume.

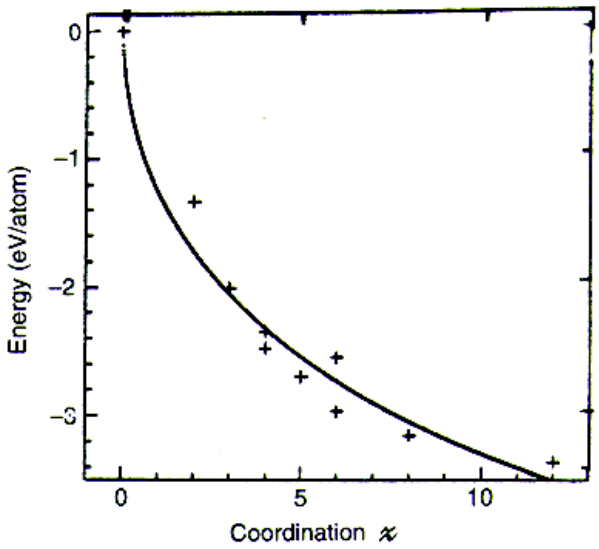

Figure 6.17: DFT-LDA cohesive energy (plotted here as a negative number) for Al as a function of the nearest neighbor coordination NN in various lattice types. The lattice types considered are the linear chain ($NN = 2$), graphite ($NN = 3$), diamond ($NN = 4$), two-dimensional square mesh ($NN = 4$), square bilayer ($NN = 5$), simple cubic ($NN = 6$), triangular mesh ($NN = 6$), vacancy lattice ($NN = 8$) and fcc ($NN = 12$). The solid curve is a fit to $A \cdot (NN) - B\sqrt{NN}$ [from V. Heine *et al.*, Phil. Trans. Royal Soc. (London) **A334**, 393 (1991)].

bonding density lies in the purely covalent Ge solid still symmetrically between the atoms, the maximum shifts more and more towards the anion for the case of the III-V and II-VI compound. GaAs can still be discussed in the sp^3 picture, e.g. as $Ga^{(-)}(4s^1 4p^3)$ and $As^{(+)}(4s^1 4p^3)$. The range of the sp^3 hybrids is, however, larger for the As anion than for the Ga cation, shifting the bonding maximum and giving the bonding a slightly ionic touch. This becomes then even more pronounced for the II-VI compound, and for the I-VII alkali halides discussed in section 6.2, the purely ionic bonding character is attained.

6.5 Metallic bonding

Although we have already viewed the even or completely one-sided sharing of electrons in covalent and ionic bonding as somewhat opposite extremes, they are similar in the sense that the valence electrons are still quite localized: either on the ions or in the bonds between the atoms. The conceptual idea behind *metallic bonding* is now complementary to this, and describes the situation, when the valence electrons are highly delocalized. In other words they are well shared by a larger number of atoms - in fact one can no longer say to which atom a valence electron really belongs: it is simply part of the "community". Such a situation is for example most closely realized in the alkali metals, which readily give away their only weakly bound s electron in the valence shell. In most abstract terms, such metals can thus be perceived as atomic nuclei immersed in a featureless electron glue. From this understanding, we can immediately (just like in the covalent case) draw a couple of conclusions:

- A delocalized binding is not directional, and should allow for easy displacement of the individual atoms with respect to each other. Metals are therefore rather elastic and ductile.

- Delocalization is the consequence of heavy overlap between the individual valence wave functions. The bands will therefore exhibit a strong dispersion, rendering the opening up of energy gaps in the density of states (DOS) less likely. With the Fermi level cutting anywhere through this gapless valence DOS, unoccupied states will exist immediately above the highest occupied one. Indeed this is the defining characteristic of a metal and application of small external perturbations, e.g. an electric field, can then induce current flow, i.e. metals are electric conductors (and in turn also good thermal conductors).

- It is intuitively clear that a contribution arising from delocalized bonding between many atoms can not be described by a sum of pair potentials. This results equally from the understanding that pair potentials are only adequate when there is a negligible distortion of the atomic electron density when the atom is added to the solid. In metals, on the other hand, the overlap between the valence wave functions is so large that the atomic character is hardly recognizable any more. That simple pair potentials will not be appropriate for the description of metallic systems is also nicely visible from plots like the one shown in Fig. 6.17. Here, the cohesive energy for Al is plotted as a function of the nearest neighbor coordination NN in various crystal lattices. If the binding arose only out of pairwise bonds with the nearest neighbors, the cohesive energy would be proportional to NN. What is instead obtained typically as in Fig. 6.17 is that the cohesive energy scales with the coordination more like $A \cdot (NN) - B\sqrt{NN}$, with A and B constant. Apparently, increasing the local coordination about a given atom reduces the strength of the existing bonds, as the delocalized electrons spread more evenly between all neighbors. This phenomenon characteristic for metallic bonding is often called *bond order conservation*, while chemists refer to an *unsaturated* nature of the metallic bond. With pure pair potentials failing, the common theme of interatomic potential schemes used for metals is therefore to add a coordination dependent term, which reduces the linear scaling due to the pair potential for higher coordinated atoms. Most famous examples of such approaches are the so-called Embedded Atom Method (EAM) or Finnis-Sinclair/Bond-Order Potentials (BOPs). Still, the same word of caution holds here as already discussed for the covalent crystals: Although frequently employed in materials sciences, there is yet no really reliable and transferable interatomic potential scheme for metals. Presumably there will never even be one, and real quantitative understanding can only come out of quantum mechanical calculations explicitly treating the electronic degrees of freedom.

As already in the case of covalent bonding, we will have to look for alternatives that will bring us a conceptual understanding of the quantitative data coming out of DFT calculations. And we will do this first for the so-called *simple* or free-electron like metals, which comprises for example the alkali and alkaline earth metals[1] (group I and II). Characteristic data for some alkalis on which we will concentrate is listed in Table 6.7. Fig. 6.18 shows

[1]Although the alkaline earth metals have a filled valence s shell, under normal conditions they are metallic solids because of partial occupation of their p bands (*sp* hybridization).

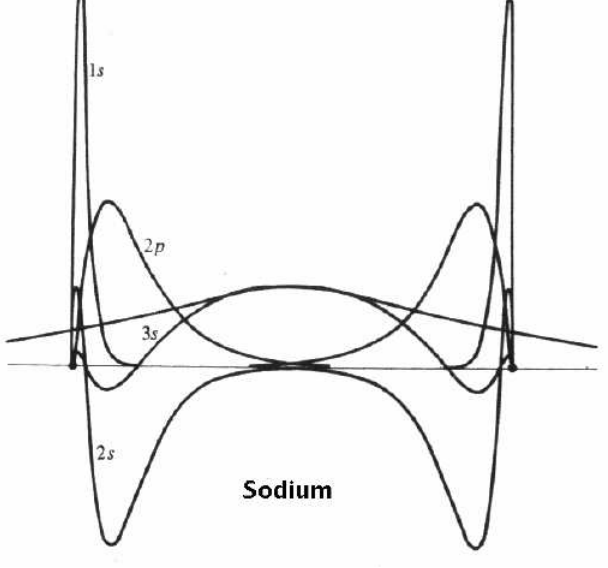

Figure 6.18: Radial wavefunctions of two sodium atoms at the equilibrium interatomic distance they would have in the crystal. There is very small overlap between the $2s$ and $2p$ orbitals, but a very large overlap of the $3s$ valence wave functions [from Ashcroft and Mermin].

Element	a_o (Å)	$E^{\rm coh}$ (eV/atom)	r_s/a_B
Li	3.49	1.63	3.27
Na	4.23	1.11	3.99
K	5.23	0.93	4.95
Rb	5.59	0.85	5.30
Cs	6.05	0.80	5.75

Table 6.7: Experimental values for structural and cohesive properties of group I alkalis in the bcc structure. a_o lattice constant, $E^{\rm coh}$ cohesive energy, and r_s the Wigner-Seitz radius.

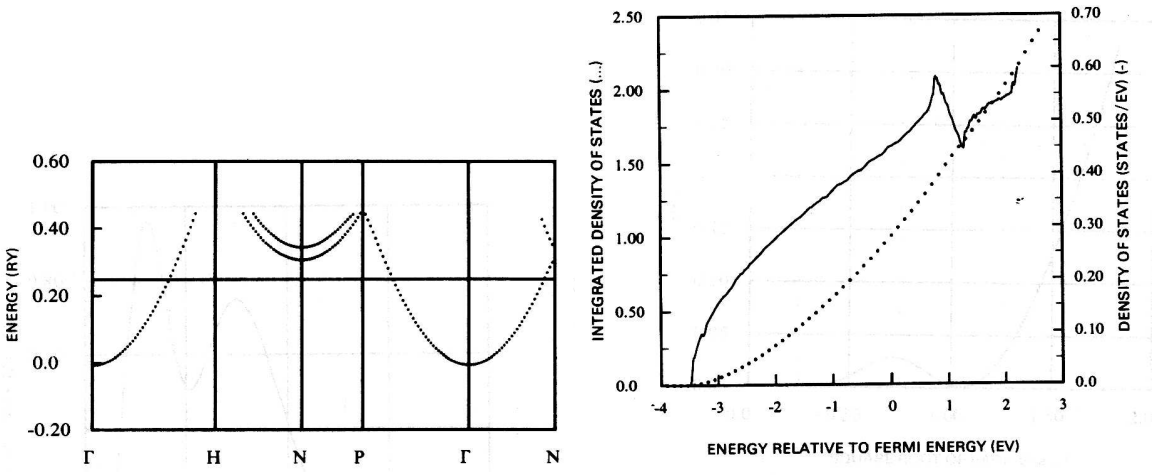

Figure 6.19: DFT-LDA Bandstructure (left) and DOS (right) for Na in the bcc structure. Note how much the valence bands follow a free-electron like dispersion, as also clearly visible in the parabolic shape of the DOS [from V.L. Moruzzi, J.F. Janak and A.R. Williams, *Calculated electronic properties of metals*, Pergamon Press (1978)].

the radial wave functions of two Na atoms at the equilibrium distance they would have in a bcc solid, from which the already mentioned strong overlap of the valence $3s$ states is apparent. In fact, ignoring the oscillations near the two nuclei, the charge distribution of the overlapping $3s$ orbitals can be seen to be practically constant. The band structure of alkalis should therefore exhibit a dispersion very similar to the one of free electrons (hence the name given to these metals), as also illustrated in Fig. 6.19 for Na. It also suggests that the simple jellium model discussed already in chapter 3 could serve as a suitable minimum model to qualitatively describe the bonding in the alkali crystals. In this jellium model, the electron density is considered to be constant over the whole solid, and in its simplest form the ion lattice is equally smeared out to a constant density exactly compensating the electronic charge. The model is then completely specified by just the electron density $n = N/V$, which is usually given in form of the so-called *Wigner-Seitz radius*

$$r_s \;=\; \left(\frac{3}{4\pi\, n}\right)^{1/3} \quad , \tag{6.28}$$

corresponding to the spherical volume available to one conduction electron. In chapter 3 we had seen, that the energy per electron can be written as

$$\begin{aligned} E/N \;&=\; T \;+\; E^{\text{ion}-\text{ion}} \;+\; E^{\text{el}-\text{ion}} \;+\; E^{el-el} \\ &=\; T_s \;+\; E^{\text{ion}-\text{ion}} \;+\; E^{\text{el}-\text{ion}} \;+\; E^{\text{Hartree}} \;+\; E^{\text{XC}} \quad , \end{aligned} \tag{6.29}$$

where T (T_s) is the kinetic energy of the (non-interacting) electron gas, $E^{\text{ion}-\text{ion}}$ and $E^{\text{el}-\text{ion}}$ the energy due to ion-ion and electron-ion interaction, and the energy due to electron-electron interaction, $E^{\text{el}-\text{el}}$, has been divided into Hartree and exchange-correlation contributions. For the completely smeared out constant ion density, one finds that

$$E^{\text{Coulomb}} \;=\; E^{\text{ion}-\text{ion}} \;+\; E^{\text{el}-\text{ion}} \;+\; E^{\text{Hartree}} \;=\; 0 \quad , \tag{6.30}$$

i.e. the Coulomb interaction due to the constant electron and ion densities cancels. This simplifies eq. (6.29), and in the exercise you will derive that one obtains for the energy in the Hartree-Fock approximation

$$(E/N)_{\text{const. ion}} \;=\; T_s \;+\; E^{\text{XC}} \;\overset{HF}{\approx}\; \frac{30.1\,\text{eV}}{\left(\frac{r_s}{a_B}\right)^2} \;-\; \frac{12.5\,\text{eV}}{\left(\frac{r_s}{a_B}\right)} \quad . \tag{6.31}$$

Interestingly, this energy exhibits a minimum at $r_s^0 = 4.8\, a_B$, i.e. already this crudest model of delocalized electrons leads to bonding. Before we directly proceed to analyze how this compares to the real alkalis (or how we may somewhat refine our toy model), let us first understand this quite astonishing fact. If we had treated the electron gas as independent particles, its energy would have only contained the kinetic energy T_s. As we can see from eq. (6.31), this first term is purely repulsive. Since in this approximation, the attractive electrostatic potential from the smeared-out ionic background is exactly compensated by the average repulsive field from all the other electrons, there is no reason for the electrons to stay closer together. Adding exchange in the Hartree-Fock approximation, however, introduces the exchange-hole around each electron as discussed in chapter 3. Due to this lowering of the electron density in its immediate vicinity, each electron sees now an additional attractive potential from the surrounding positive jellium background. Since

fcc	hcp	bcc	sc	diamond
1.79186	1.79175	1.79168	1.76012	1.67085

Table 6.8: Madelung constants for ion lattices immersed in a compensating constant electron density [from C.A. Sholl, Proc. Phys. Soc. **92**, 434 (1967)].

the potential at the centre of a sphere of uniform charge varies inversely with the sphere radius, we expect the electron to feel an additional attractive potential proportional to $1/r_s$. This is indeed the second term in eq. (6.31), lowering the energy and leading to a binding minimum.

Having understood this, how good or bad are we actually doing with this jellium model? The alkalis crystallize in the bcc structure, which is something we cannot get out of our present model, because we have neglected the explicit form of the crystalline structure (but we will comment on the bcc structure below). The alkali atoms have one valence s electron, i.e. the number of electrons N is equal to the number of atoms M in the system. With this, we obtain for the cohesive energy

$$E^{\rm coh} \;=\; -\left(\frac{E[r_s^0]}{M} \;-\; \frac{E[r_s\to\infty]}{M}\right) \;=\; -\frac{E[r_s^0]}{N} \;=\; 1.3\ {\rm eV/atom} \quad . \tag{6.32}$$

And in the bcc lattice with one electron per atom, the Wigner-Seitz radius is related to the lattice constant by $a_{\rm bcc} \approx 1.1(r_s/a_B)$. We therefore obtain for the lattice constant $a^0_{\rm bcc} = 5.3\,$Å. Comparing these two cohesive quantities with the data compiled in Table 6.7, the success of this admittedly trivial model is impressive.

In particular, since we are well aware that we are looking at a spitting image of reality, we should verify that this agreement is not fortuitous. First, one should check, whether the Hartree-Fock approximation does really already describe the major effect due to the electron-electron interaction. For the simple jellium system, one can fortunately calculate the correlation beyond Hartree-Fock rather well. From homogeneous electron gas theory we therefore find that such further contributions lead to a lowering of the equilibrium Wigner-Seitz radius from $r_s^0 = 4.8\,a_B$ to $4.23\,a_B$ (and increasing the cohesive energy to $2.2\,$eV/atom), i.e the HF value was not too bad after all. On the other hand, the other most drastic approximation in our model was to smear out the ion lattice to a constant value. Alternatively, one can employ a lattice of point charges with $Z = e$ (for the alkalis) to resemble the atomic nuclei. Then, the Coulomb interaction of eq. (6.30) between electrons and ions does not cancel anymore. Instead one obtains (e.g. C.A. Sholl, Proc. Phys. Soc. **92**, 434 (1967))

$$E^{\rm Coulomb} \;=\; -\frac{\alpha}{2}\,\frac{e^2}{r_s} \quad , \tag{6.33}$$

where α is again a Madelung constant. This time it refers to positive ions immersed into 1 constant electron density. Values for α for some lattices are given in Table 6.8. Considering the ion lattice explicitly leads therefore to another term lowering the electron energy (negative sign!), which is lowest for the lattice maximizing the Madelung constant. This lattice would correspondingly result as the stable one in our model, but looking at the values listed in Table 6.8 we find that we will be unable to distinguish between fcc, hcp and bcc lattices. That the two close-packed lattices are among the most stable is no real

surprise, but the high stability of the more open bcc lattice is interesting. From the non-directionality of the metallic bond, we would have intuitively expected the close-packed lattices to be most favorable. Yet, even if this was so, our analysis shows now that the bcc lattice will be not very much less favorable (and this also results from accurate DFT calculations of the alkalis). Since entropy favors more open structures, a phase transition to bcc could therefore already occur at very low temperatures. At the finite temperatures at which experiments have been carried out to date, always the bcc structure is found for all alkali metals. Whether this is really the ground state structure, or just the result of a lowest temperature phase transition is not yet understood.
In any case, in the bcc structure the Coulomb interaction term becomes

$$E^{\text{Coulomb}} = -\frac{24.4\,\text{eV}}{\left(\frac{r_s}{a_B}\right)} \quad . \tag{6.34}$$

Adding this to eq. (6.31), we now obtain as the minimum $r_s^0 = 1.6\,a_B$, i.e. the new energy lowering term has considerably shifted the optimum for metallic binding to higher electron densities. In fact, the shift is so large, that we now obtain a way too small lattice constant of 2.7 Å, cf. Table 6.7. The reason for this overshooting in the correction compared to the smeared-out ion result is also the reason why in both cases we erroneously obtain identical lattice constants and cohesive energies for *all* alkali metals (there is no "material dependence" in the optimum electron density). Instead of point-like ions, there will in reality be a finite core region with a high density of core electrons. Due to exchange and correlation, the valence electrons will be repelled from this region and will be confined to a smaller region left in between. This increases the average electron density in this region and thus also the kinetic energy repulsion. In parallel, the valence electrons can also not come as close to the positively charged ions as in the situation approximated by the point-like lattice. This gives less negative electrostatic energy, i.e. in total both the exchange and the kinetic energy term will favor $r_s > 1.6$ (lower densities), when finite core regions are considered. Depending on the size of the core region, one will therefore describe the alkali better with either the smeared-out ion model (approximating a large core region) or with the point-like ion model (approximating a small core region). This also explains the varying cohesive values within the alkali metal series: The small core region of Li is still very well modelled by the point-like lattice model, whereas the large core region of the heavy Rb or Cs approach already the situation described better by our original smeared-out ion model.
This correspondence is in fact exploited semi-quantitatively by assigning so-called *empty-core (or Ashcroft) pseudopotentials* to each metal, such that a jellium model on the level as discussed above (but with a finite impenetrable core region corresponding to the empty-core radius) fits the experimental cohesive data (lattice constant, cohesive energy) best. Although this allows to describe quite a range of properties ranging from phonon spectra and optical absorption to superconducting transition temperatures for all simple metals, this refinement is not very instructive for our general discussion on bonding. For us, it is primarily important that we understand that delocalized electrons can lead to metallic bonding. On the other hand, what we can not yet understand on the basis of our crude model (in fact not even with the refinement of empty-core pseudopotentials), is why the *transition metals* (TMs) exhibit significantly higher cohesive energies than the simple metals (W has the highest one with 8.9 eV/atom). Furthermore, why do the cohesive properties follow roughly a parabolic pattern over one transition metal series as

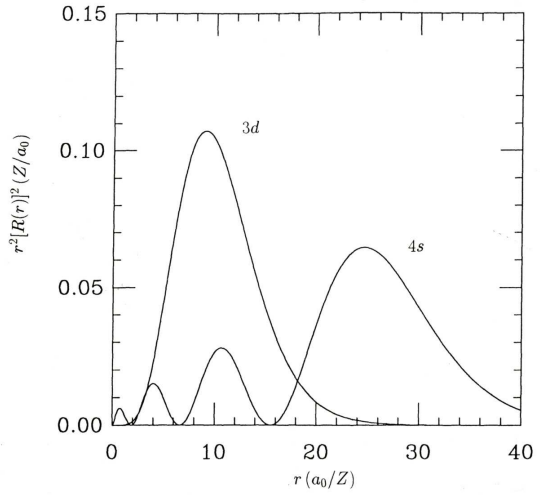

Figure 6.20: Typical radial distributions of the valence $3d$ and $4s$ wavefunctions in a $3d$ transition metal. Compared to the s states the d states are much more contracted [from C.S. Nichols, *Structure and Bonding in Condensed Matter*].

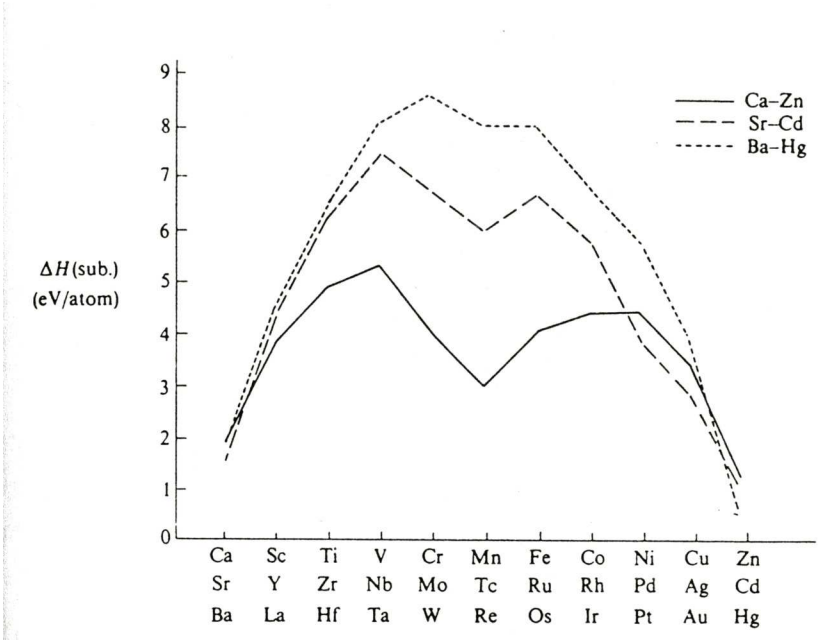

Figure 6.21: Experimental heat of formation for the $3d$, $4d$ and $5d$ transition metals. A parabolic variation of the cohesive properties is clearly visible for the $4d$ and $5d$ metals. For the $3d$ series this trend is less clear, as discussed in the text [from C.S. Nichols, *Structure and Bonding in Condensed Matter*].

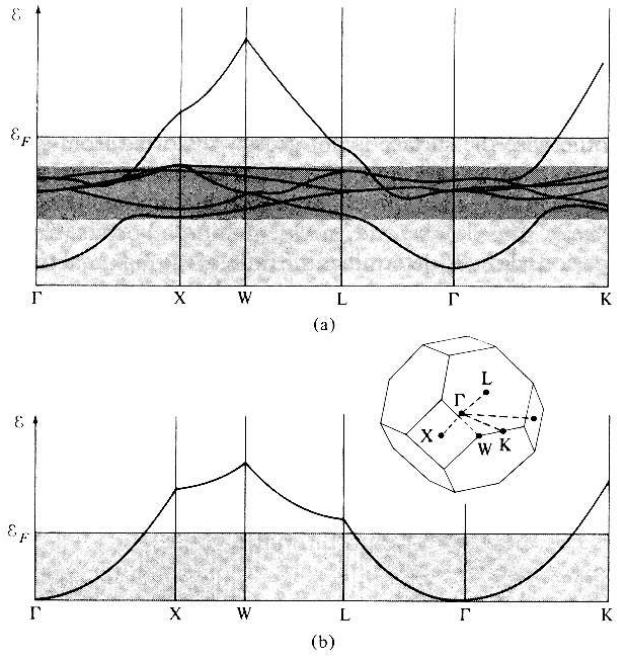

Figure 6.22: DFT-LDA band structure for Cu in the fcc structure (upper panel). The s bands are located in the region shaded in light grey and show a dispersion highly reminiscent of free electrons (the band structure of which is shown in the lower panel for comparison). In contrast, the bands deriving from the d orbitals (lying in the dark shaded region) are rather flat and have no correspondence in the free electron band structure [from Ashcroft and Mermin].

exemplified in Fig. 6.21, which is furthermore accompanied by a systematic change of stable crystal structure from bcc over hcp to fcc when going from early to late TMs? There must be another component in the bonding responsible for this, and it is not difficult to imagine that this has to do with what is special about the TMs, namely the partly filled d valence shell. These stats add to the metallic bonding a strong covalent contribution.
In a general, but highly simplified view, the d-orbitals can be regarded as relatively strongly localized compared to the s valence electrons of the simple metals. A "tight-binding" type description in the sense of atomic-like orbitals is then reasonable, even in the solid. Compared to the delocalized s bands, the d bands will correspondingly be rather flat, as can indeed be seen in the band structure of Cu shown in Fig. 6.22. The valence density of states for transition metals can therefore be schematically decomposed into two contributions: a broad, featureless and essentially parabolic part due to the valence s states (comparable to the simple alkali metals) *and* a relatively narrow (few eV wide) part due to the d states as illustrated in Fig. 6.23. Since there are many more d states than s states, the d contribution dominates, and the varying (cohesive) properties over a transition metal series can essentially be understood from a differing degree of filling of the d band ("rigid band model"): the number of valence electrons increases over the TM series (e.g. Ru 8, Rh 9, Pd 10, and Ag 11 valence electrons), shifting the Fermi level more and more to the right within the d band dominated DOS. At the end of a TM series, the d band is finally completely filled and the Fermi level cuts through the again s-like part of the DOS above the d band, as can e.g. be seen in the band structure of Cu shown in

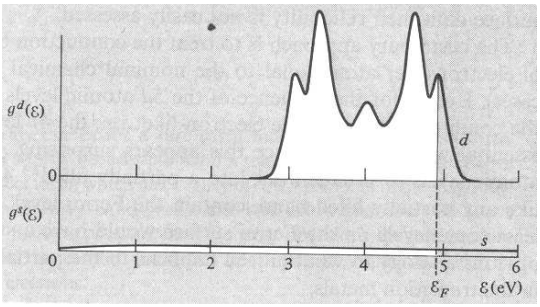

Figure 6.23: Qualitative p (fcc) density of states (DOS): a wide featureless ow, structured d band. Due to the larger numbe: o the DOS dominates, and the varying propertie: arising from a differing degree of filling of the d ba Ashcroft and Mermin].

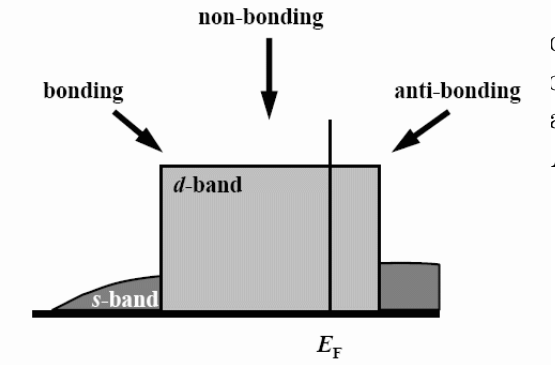

Figure 6.24: Density of states in the rectangular d band model for transition metals.

Fig. 6.22. Such transition metals with completely filled d bands are called *noble metals* (Cu, Ag, Au).

The simplest model reflecting this understanding of the TM valence electronic structure as a composition of nearly free electron s bands and "tight-binding" d bands is the so-called *rectangular d band model* of Friedel. Here, the s states are taken as free-electron like (i.e. the jellium model discussed for the simple metals) and the d states as constant over a given band width W as sketched in Fig. 6.24. Within this simple model one can analytically derive and understand surprisingly many, not only cohesive properties of TMs, and we will encounter it again in later chapters of this lecture. Here, we content ourselves with discussing only the salient features with respect to cohesion qualitatively. Due to the more localized nature of the d orbitals, their bonding contribution is in fact more covalent than metallic. Bringing the atoms closer together results in d wave function overlap and a splitting into bonding and antibonding states yielding the narrow d band. Within this d DOS we therefore expect the lowest energy states to exhibit a more bonding character, followed by non-bonding states at intermediate energies and the highest energy states to be of antibonding character.

What does this understanding now mean for the cohesive properties? Going over one TM series, we start with the early transition metals and accordingly begin to fill electrons into the lowest energy d states. These are of bonding type and we expect an increase in the cohesive energy. Since the DOS is dominated by d states, this rise in cohesion should be rather strong, too. Due to the shorter range of the d orbitals, their bonding contribution will also favor smaller lattice constants to maximize the wave function overlap. Towards the middle of the TM series the solids should therefore exhibit strongly increasing cohesive energies and decreasing lattice constants. The packing fraction and corresponding s

electron density becomes then higher than the optimum r_s for the metallic bonding (e.g. compare the bcc lattice constants around 3 Å of the 5B and 6B TMs (V, Cr, Nb, Mo, Ta) with the $\sim$ 5 Å favored by the heavy alkalis of similar core radius). The resulting structure and cohesion balances therefore a contractive tendency from the d orbitals with a repulsive tendency from the s electron gas (often called *s pressure*). Once the filling reaches the non-bonding and anti-bonding higher energy states in the d band (i.e. for the middle and late TMs), the increasing number of d electrons does not yield further bonding anymore, and even diminishes the existing one. The cohesive energy will level off and decrease, while the s pressure leads to increasing lattice constants. At the noble metals, the d contribution has in this simplistic view finally cancelled completely, and we reobtain cohesive properties (very roughly only) comparable to the simple metals. Calculating through the rectangular d band model, one obtains therefore in total a parabolic shape for the cohesive energy over a TM series, and using the really computed d band widths of the order of a few eV for the parameter W, also the absolute magnitude of the cohesive energy comes out very well.

With a very crude model we can therefore (again) understand the qualitative cohesive trend over a large number of elements. What we can not reproduce with it yet, but which is something that comes out very well in state-of-the-art DFT calculations by the way, is the structural trend from bcc to hcp to fcc over the TM series and the strange dip at the top of the parabola in the middle of the TM series, cf. Fig. 6.21. The first point can obviously not be understood within the rectangular d band model, since there is no explicit lattice structure contained in it. When one considers the latter, say in DFT calculations, one finds that the lattice affects the sub structure within the d DOS that is apparent in Fig. 6.23, but neglected in the coarse rectangular d band model. One can understand this sub structure in the DOS directly from the band structure: The DOS results from the integration over the Brillouin zone; points that occur often and where the bands are relatively flat, will thus give rise to a high density of states. For the fcc lattice, cf. Fig. 6.23, one would for example typically expect five peaks, three associated with the (eightfold occurring) L point and two with the (sixfold occurring) X point, cf. Fig. 6.22. The shape of the d DOS is in other words quite characteristic for a given lattice type, not so much for the element (which more dictates the *filling* of the d DOS, again in the view of the "rigid band model"). Comparing this characteristic shape for bcc, hcp and fcc structures one can discern e.g. a rather skewed form of the bcc d DOS with many low lying states. All three lattices (bcc, fcc, hcp) offer almost the same volume per atom, in which case one can show that the contribution from the single particle energies governs the final total energy [H.L. Skriver, Phys. Rev. B **31**, 1909 (1985)]. If a particular lattice structure offers therefore an optimum number of bonding states for a given filling fraction (like the bcc structure for small fillings), it will result as most stable. With the characteristic DOS shapes, we therefore obtain in all three TM rows the same sequence bcc $\rightarrow$ hcp $\rightarrow$ fcc depending on the filling ratio (a more in depth discussion of this point can for example be found in D. Pettifor, *Bonding and Structure of Molecules and Solids*, Clarendon Press (1995)).

This leaves as the last point the dip in the middle of the TM series, cf. Fig. 6.21 The reason behind this is the special properties of the free atoms that the cohesive energy results as the difference between the energy of the isolated atom and the solid!). or atoms in the center of the TM series. In particular for Mn ($3d^5 4s^2$) and Mo ($4d^5 5s^1$), the $d-d$ correlation is particularly important and leads to a pronounced stability of the isolated

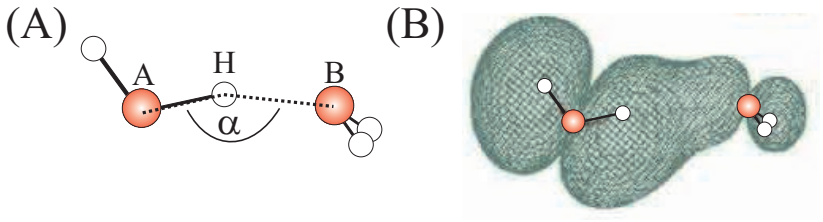

Figure 6.25: (A) The structure of the water dimer, which illustrates the structure of a typical H bond. (B) An isosurface of constant electron density for one of the occupied molecular orbitals in the water dimer, illustrating overlap between the wavefunctions of both water molecules in the dimer. B is taken from http://www.lsbu.ac.uk/water/index.html, a very informative and detailed website on the properties of water.

atom. In the solid this is less important, i.e. there is no unusual stability compared to the overall TM trend, yielding in total a diminished cohesive energy for these elements and a dip in the parabola.

6.6 Hydrogen bonding

The final type of bonding that we shall briefly discuss is 'hydrogen bonding'. Here we shall provide little more than a basic introduction. More information can be found in, for example, *Theoretical treatments of hydrogen bonding*, edited by Dusan Hadzi or An Introduction to H bonding by G.A. Jeffrey.
The importance of hydrogen bonds to the structures of materials can scarcely be overstated. Hydrogen bonds are the single most important force determining the three dimensional structure of proteins, the structure of liquid water and in the solid state they feature most prominently in holding the water molecules in ice together. Indeed it has been estimated that a paper related to H bonding is published on average every fifteen minutes (see G.A. Jeffrey, *An Introduction to H bonding*).
The concept of some special hydrogen mediated interaction has been around since 1902 when Werner examined the reaction of ammonia and water. Not since the work of Latimer and Rodebush in 1920, however, has this interaction been known as a hydrogen bond[2].
Generally *H bonds form when a covalently bound H atom forms a second bond to another element*. Schematically the H bond is often represented as A-H...B. A will invariably be an em electronegative species (for example N, O, F, Cl) and B must be an electron donor. The structure of a typical H bond, the H bond in the water dimer, is shown in Fig. 6.25.

6.6.1 Some Properties of Hydrogen bonds

Several properties of the H bond are clear:

- Although H bonds are the strongest intermolecular forces, compared to covalent or ionic bonds they are relatively weak. H bond strengths range from about 0.1 eV to

[2]Huggins contests this, claiming that the he proposed the H bond in 1919 - see G.A. Jeffrey, *An Introduction to H bonding*, for an interesting discussion on the history of H bonds.

0.5 eV. Water-water H bonds in ice or the water dimer are of intermediate strength, generally around 0.25 eV.

- H bonds are directional with A-H-B angles close to 180°. Indeed the stronger the H bond the closer it will be to 180°.

- Upon formation of a H bond the AH bond (generally termed the H bond donor) is lengthened slightly, by about 0.01-0.04 Å. This leads to softened ('red-shifted') and broadened AH vibrations, which can be observed by experiment. Indeed the lengthening of the AH bond upon formation of a H bond correlates with the magnitude of the red-shift and also correlates with the A-B distance. See Fig 6.26 for an illustration of this effect.

- H bonds can be 'cooperative'. In general this means that the strength of H bonds amongst fragments may *increase* as more H bonds are formed. Indeed several H bonded chains such as the boron hydride polymer or a helix of alanine molecules show a monotonic cooperative increase. Specifically the average H bond strength between monomers chain increases as the chain lengthens:

$$E_2 < \overline{E}_3 < \overline{E}_4 < ... < \overline{E}_N < ... < \overline{E}_\infty \tag{6.35}$$

  The cooperative enhancement of infinite chains is typically quantified by the dimensionless fraction: $\overline{E}_\infty/\overline{E}_2$. Cooperative enhancements can be large, for example, recent calculations predict a cooperative enhancement factor of >2 , for the alanine chain. This is a dramatic cooperative increase in H bond strength. This cooperative behaviour of H bonds is the opposite of the more intuitive behaviour exhibited by, for example, covalent bonds which generally *decrease* in strength as more bonds are formed (cf. Fig. 6.21). Cooperativity of H bonds is a crucial physical phenomena in biology, providing additional energy to hold certain proteins together under ambient conditions.

6.6.2 Some Physics of Hydrogen bonds

Although many of the structural and physical properties of H bonds are clear, the electronic make-up of H bonds is less clear and remains a matter of debate. The unique role H plays is generally attributed to the fact that the H ion core size is negligible and that H has one valence electron but unlike the alkali metals, which also share this configuration, has a *high* ionization energy. Generally it is believed that H bonds are mostly mediated by electrostatic forces; stabilized by the Coulomb interaction between the (partial) positive charge on H and the (partial) negative charge on the electronegative element B. However, H bonds are *not purely* electrostatic. First, it has been shown that for the water dimer (the most studied prototype H bond) it is not possible to fit the energy versus separation curve to any of the traditional multipole expansions characteristic of a pure electrostatic interaction (see S. Scheiner, *Hydrogen bonding a theoretical perspective*, for more details.). Second, first- principles calculations reveal overlap between the wavefunctions of the donor and acceptor species in the H bond. This is shown in Fig. 6.25(B) which shows one of the occupied eigenstates of the gas phase water dimer. Overlap between orbitals such as

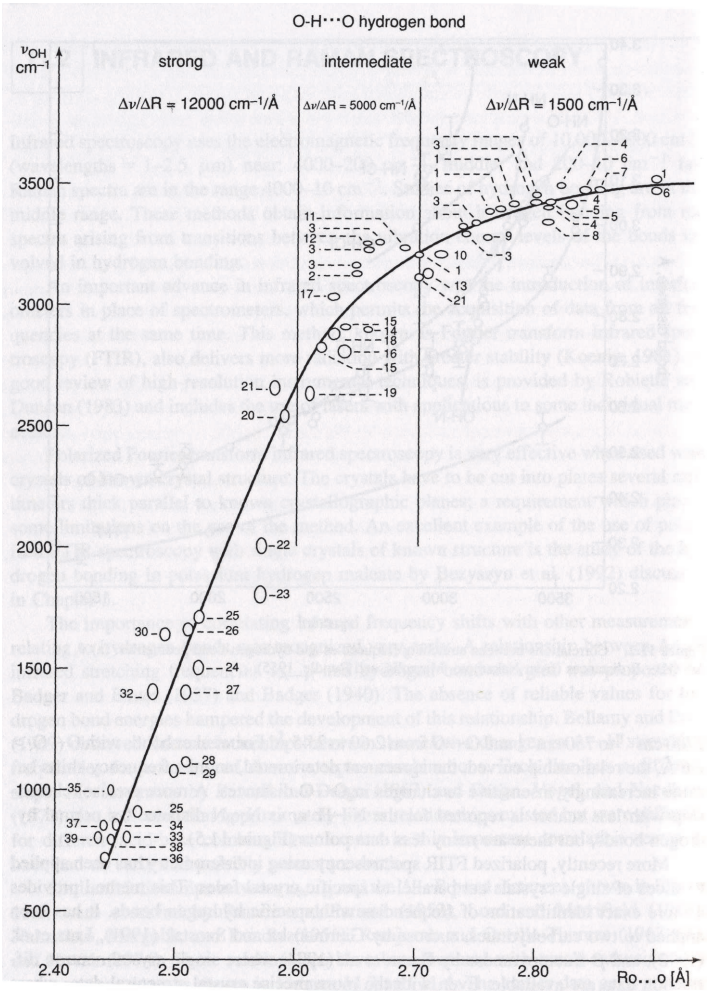

Figure 6.26: Correlation between the A-B distance (in this case O-O distance) and OH vibrational frequency for a host of H bonded complexes. From G.A. Jeffrey, *An Introduction to H bonding*.

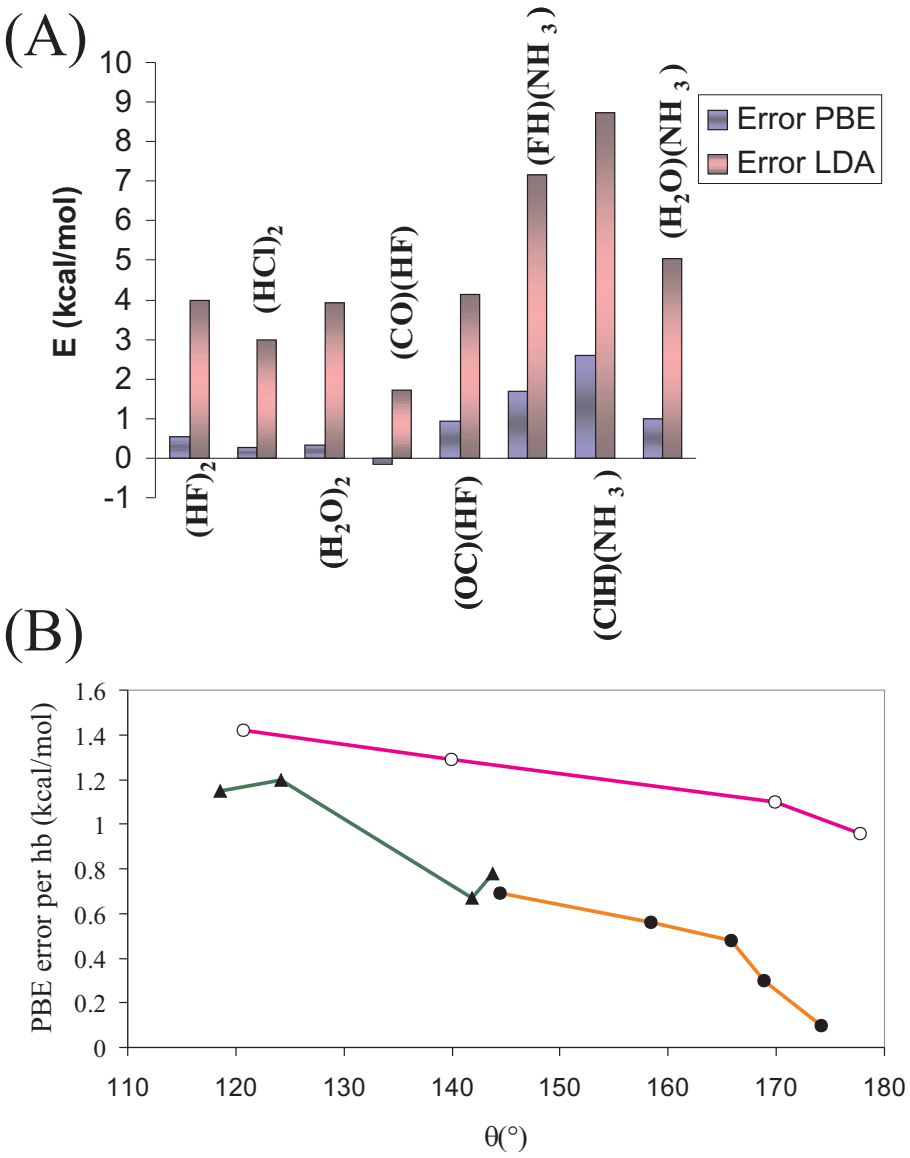

Figure 6.27: (A) Comparison between LDA and GGA error for H bond strengths in several gas phase complexes (from C. Tuma, D. Boese and N.C. Handy, Phys. Chem. Chem. Phys. 1, 3939 (1999)) (B) Correlation between PBE error and H bond angle for several gas phase H bonded complexes. See J. Ireta, J. Neugebauer and M. Scheffler J. Phys. Chem. A 108, 5692 (2004) for more details.

that shown in Fig. 6.25(B)is characteristic of covalent bonding. Current estimates of the electrostatic contribution to a typical H bond range anywhere from 90 to 50%.
Finally, we shall end with a brief discussion on how well DFT describes H bonds. This question has been tackled in countless papers recently, particularly by focussing on the H_2O dimer and other small gas phase clusters. The two most general (and basic) conclusions of these studies are:

- Predicted H bond strengths strongly depend on the exchange correlation functional used. The LDA is *not* adequate for describing H bonds. The LDA routinely predicts H bonds that are too strong by 100%. GGAs on the other hand generally predict H bond strengths that are close (within 0.05 eV) of the corresponding experimental value. This general conclusion is summarised nicely in Fig. 6.27(A) which plots the difference between DFT (LDA and GGA (PBE)) H-bond strengths from those computed from high level quantum chemical calculations (post Hartree-Fock methods such as Configuration Interaction or Coupled-Cluster, which can yield almost exact results) for several gas phase H-bonded clusters. It can be seen from this figure that LDA always overestimates the H bond strengths, by at least 4 kcal/mol (0.16 eV). PBE on the other hand is always within 1 kcal/mol (0.04 eV) of the 'exact' value.

- The quality of the GGA (PBE) description of H bonds depends on the structure of the H bond under consideration. Specifically, it has been shown that the more linear the H bond is, the more accurate the PBE result is. This is shown in Fig. 6.27(B) for several different H bonded gas phase clusters.

6.7 Summary

Some of the key features of the five main types of bonding are shown in Fig. 6.28.

Type	Schematic	Cohesive Energy	Examples
Van der Waals	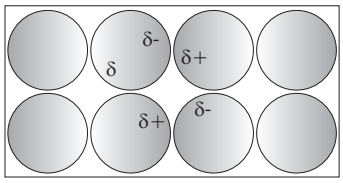	very weak: 1-10 meV	noble gases (Ar, Ne, etc), organic molecules
H bonding	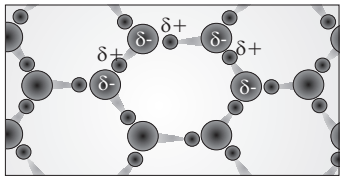	weak: 0.1-0.5 eV	water, ice, proteins
Covalent	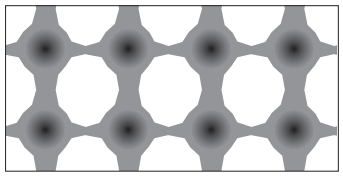	strong: ≤11 eV (molecules) ≤8 eV (solids)	C (graphite, diamond), Si, transition metals
Metallic	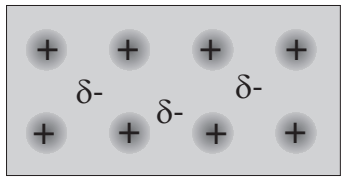	strong: ≤9 eV	Na, Al, transition metals
Ionic	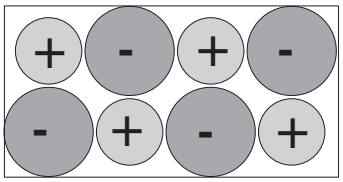	strong: ≤8 eV	NaCl; NaBr, KI

Figure 6.28: *Very* simple summary of the main types of bonding in solids